Journal of Radiation Research and Applied Sciences 18 (2025) 101989

Contents lists available at ScienceDirect

Journal of Radiation Research and Applied Sciences

journal homepage: www.journals.elsevier.com/journal-of-radiation-research-and-applied-sciences

AI-driven design and optimization of microwave radiation-induced pyrolysis systems using machine learning and metaheuristic algorithms

Narinderjit Singh Sawaran Singh [a], Rashid Khan [b], As'ad Alizadeh [c,*], Mohamed Shaban [d,**], Mazen M. Othayq [e], Abdellatif M. Sadeq [f], Husam Rajab [g], Joy Djuansjah [b]

[a] Faculty of Data Science and Information Technology, INTI International University, Persiaran Perdana BBN, Putra Nilai, Nilai, 71800, Malaysia
[b] College of Engineering, Imam Mohammad Ibn Saud Islamic University (IMSIU), Riyadh, Saudi Arabia
[c] Department of Civil Engineering, College of Engineering, Cihan University-Erbil, Erbil, Iraq
[d] Department of Physics, Faculty of Science, Islamic University of Madinah, Madinah, 42351, Saudi Arabia
[e] Department of Mechanical Engineering, College of Engineering and Computer Sciences, Jazan University, Jazan, 45112, Saudi Arabia
[f] Mechanical and Industrial Engineering Department, College of Engineering, Qatar University, Doha, Qatar
[g] College of Engineering, Department of Mechanical Engineering, Najran University, King Abdulaziz Road, P.O Box 1988, Najran, Saudi Arabia

ARTICLE INFO

Keywords:
Radiation-assisted pyrolysis
Biomass conversion
Machine learning
Energy efficiency
Grey wolf optimizer
MCDM

ABSTRACT

Microwave radiation-assisted pyrolysis holds significant promise for sustainable biomass valorization, yet effectively modeling and optimizing this complex radiation-driven process remains challenging due to its inherent nonlinearity and multi-dimensional trade-offs. This study addresses this critical gap by proposing an innovative hybrid framework that integrates advanced machine learning, metaheuristic multi-objective optimization, and systematic multi-criteria decision-making. The primary objective was to holistically model, optimize, and prioritize operating scenarios for microwave radiation-induced pyrolysis of palm kernel shells (PKS) to enhance bio-char yield and quality. The methodology combines four phases: comprehensive input–output analysis, predictive surrogate modeling using the COMBI algorithm, Pareto-based optimization via the multi-objective grey wolf optimizer (MOGWO), and final solution ranking using the weighted Tchebycheff method (WTM). The COMBI models demonstrated excellent predictive accuracy, with all objectives achieving an R^2 greater than 0.99, ensuring robust generalization and reliability. Optimization outcomes revealed insightful trade-offs among reaction time, sample mass, and nitrogen gas flow rate. Notably, higher calorific values (up to 31 MJ/kg) were achieved with shorter reaction times (≈39–40 min), smaller sample masses (≈21–23 g), and lower nitrogen flows (≈100 mL/min), whereas maximizing fixed carbon content (up to 67.6 wt%) required longer reaction times (≈42–43 min), larger feedstock quantities (≈29–30 g), and higher gas flow rates (≈140–155 mL/min). Analysis of the Pareto front showed that over 55 % of optimal solutions favored shorter reaction durations, while nitrogen flow optimization consistently converged on low to medium ranges. Final ranking using WTM yielded ten distinct decision scenarios, each aligning with different technical and practical objectives. This flexibility highlights the framework's real-world applicability, offering a robust decision-support toolkit that enables practitioners to dynamically align pyrolysis operations with shifting market demands, energy efficiency goals, and environmental constraints.

1. Introduction

The escalating accumulation of biomass residues poses both an environmental burden and a missed opportunity for advancing sustainable development goals (SDGs), particularly those addressing responsible consumption, climate action, and affordable clean energy (Jha et al., 2024). Integrated biorefinery concepts highlight that these residues should not be treated as waste but rather as resources that can be converted into high-value products within a circular bioeconomy, thereby minimizing emissions and maximizing resource efficiency (Marzban et al., 2025). Among these residues, palm kernel shell (PKS) represents a notable agricultural by-product generated in vast quantities

* Corresponding author.
** Corresponding author.
E-mail addresses: asad.alizadeh2010@gmail.com, asad.alizadeh@cihanuniversity.edu.iq (A. Alizadeh), mssfadel@iu.edu.sa (M. Shaban).

https://doi.org/10.1016/j.jrras.2025.101989
Received 17 July 2025; Received in revised form 20 September 2025; Accepted 24 September 2025
Available online 3 October 2025

by the palm oil industry (Kaniapan et al., 2021). Despite its significant carbon-rich composition, PKS is frequently underutilized or improperly managed, often relegated to open burning or inefficient disposal methods that exacerbate greenhouse gas emissions (Divyabharathi et al., 2024). Recent studies also show that coupling thermochemical valorization with carbon capture offers the potential for net-negative emissions, further enhancing the environmental benefits of waste-to-energy pathways (Kiehbadroudinezhad et al., 2025). Conventional pyrolysis methods, though widely applied for converting biomass to valuable products like bio-char and bio-oil, are hindered by drawbacks such as prolonged processing times, uneven heat transfer, and suboptimal energy conversion efficiencies, which limit their viability as a truly sustainable waste-to-energy solution (Paudel et al., 2024). In response, microwave-assisted pyrolysis (MAP) has gained increasing attention as a technologically advanced alternative capable of overcoming these limitations (Alvarado Flores et al., 2022). By employing volumetric heating, this approach ensures rapid and uniform thermal decomposition, which not only enhances process efficiency but also improves the quality and yield of the resulting char products (Lee et al., 2020). These advantages align strongly with the broader aims of the SDGs by promoting circular resource utilization and offering pathways for cleaner, more resilient energy systems derived from renewable waste streams like PKS (Blair et al., 2021).

Several studies have investigated the potential of MAP for valorizing PKS or similar biomass, consistently demonstrating its clear advantages over conventional thermal methods. For instance, Sulong et al. (Sulong et al., 2020) highlighted how MAP of PKS can efficiently produce pyroligneous acid with valuable antioxidant properties, demonstrating effective conversion and functional product potential. Meanwhile, An et al. (An et al., 2020) showcased that catalytic reforming of PKS pyrolysis vapors using microwave radiation-induced heating boosts the production of phenol and hydrogen due to enhanced deoxygenation pathways, thus improving product selectivity and energy recovery. Similarly, Idris et al. (Idris et al., 2022) demonstrated that MAP allows flexible control over char yield and calorific value when processing oil palm biomass, achieving high solid fuel quality under optimized conditions. Moreover, Ang et al. (Ang et al., 2020) found that MAP can rapidly convert PKS into carbon dots with high photoluminescent efficiency, implying that microwave radiation-induced energy input effectively shortens process time while delivering high-value nanomaterials. Furthermore, Saleh et al. (Saleh et al., 2023) compared MAP with conventional heating for hydrothermal liquefaction of PKS, showing that MAP achieves higher bio-oil yields within shorter residence times and at lower energy inputs. Hamzah et al. (Mohd Hamzah et al., 2022) advanced this field by reporting that microwave radiation-induced pyrolysis of PKS generates fractions with potent antioxidant and wound healing properties, demonstrating how MAP's rapid heating promotes the formation of bioactive compounds. Taken together, these studies consistently reveal that MAP offers tangible benefits (higher product yields, lower energy demands, and reduced processing times) making it a superior and cleaner technology for valorizing PKS and similar biomass.

However, effectively designing and optimizing MAP systems for PKS or other types of biomass requires deep insight into the intricate and inherently nonlinear interactions among multiple process parameters and product qualities (Ethaib et al., 2020). Conventional empirical or analytical approaches often fall short in capturing the complex thermochemical phenomena involved, resulting in suboptimal design choices and unpredictable performance outcomes (Siddique et al., 2022). As MAP processes are influenced by multiple intertwined variables such as reaction time, feedstock mass, and gas flow rates (each dynamically affecting thermal decomposition pathways and product distributions) accurate predictive capabilities become indispensable for systematic improvement (Syed et al., 2023). In this regard, the integration of advanced computational tools, particularly artificial intelligence (AI) and machine learning (ML) algorithms, provides a robust alternative to traditional trial-and-error experimentation (Liu et al., 2024a). These data-driven techniques are capable of mapping hidden patterns and nonlinear correlations within large datasets, enabling the development of surrogate models that can forecast output responses with high precision (Ke et al., 2024). One of the leading ML methods, artificial neural networks (ANNs), recently has played a pivotal role in accurately modeling complex nonlinear relationships. Sharma et al. (Sharma et al., 2024, 2025a, 2025b; Sharma and Sharma, 2025a, 2025b), Pattnaik et al. (Pattnaik et al., 2025), and Kumar et al. (Vinay Kumar et al., 2025) demonstrate their effectiveness in capturing intricate system dynamics and enhancing predictive accuracy. By utilizing ML-based regression frameworks, researchers can not only reduce experimental workload but also gain reliable guidance for optimizing process conditions and improving product yields (Raje et al., 2024). Ultimately, such intelligent modeling tools strengthen the decision-making foundation for engineers and designers, bridging the gap between theoretical research and scalable, energy-efficient biochar production systems designed for sustainable biomass utilization.

Several researchers have successfully applied advanced AI and ML frameworks, to tackle the intricate multi-variable modeling challenges inherent to microwave radiation-induced pyrolysis systems. For example, Yang et al. (Yang et al., 2022) demonstrated that ML can accurately model both the quantity and quality of biochar, bio-oil, and syngas from biomass MAP, achieving high predictive accuracy and highlighting the role of operating temperature and microwave power as key factors. Likewise, Shen et al. (Shen et al., 2022) showed that a suite of ML techniques, including gradient boosting and bagging regressors, excel at predicting multiple pyrolysis product yields simultaneously, supporting robust multi-output modeling for various biomass types. Meanwhile, Chen et al. (Chen et al., 2024) pioneered the integration of large language models with neural networks to optimize sawdust MAP, marking an innovative hybrid approach for data-driven multi-output prediction and process insight.

In another comprehensive review, Palla et al. (Palla et al., 2024) emphasized how ML can solve complex multivariate challenges in MAP by minimizing costly experiments and enabling robust parameter tuning. This is echoed by Ren et al. (Ren et al., 2022), which stressed that metaheuristic optimization coupled with advanced ML can fine-tune microwave radiation-induced heating and catalytic strategies to maximize energy efficiency and product quality in biomass MAP. Zhong et al. (Zhong et al., 2024) compared ANN, SVM, and random forests for predicting pyrolysis kinetics and thermodynamics from thermogravimetric data, finding RF models the most interpretable for multi-parameter predictions. Additionally, Liu et al. (Liu et al., 2024b) explored kinetic interactions in MAP, using advanced modeling to decode how biomass components influence product yields, thus supporting process design through intrinsic mechanism insights. Jiang et al. (Jiang et al., 2024) further detailed how MAP can be optimized through AI-driven reaction efficiency improvements and catalyst selection, pointing out that integrating ML with catalytic design is crucial for upgrading complex biomass feedstocks. Furthermore, ML and AI have demonstrated significant potential in other thermal radiation-based studies (Alotaibi et al., 2025; Alwadai et al., 2024; Elhaie et al., 2025; Snoussi et al., 2025), highlighting their valuable role and underscoring the need for these pioneering tools in radiation-based pyrolysis systems. These works underline how coupling ML, AI, and metaheuristic optimization significantly advances the modeling and upscaling of biomass pyrolysis, while cutting experimental costs and boosting process efficiency.

As highlighted in prior studies, several researchers have successfully applied advanced AI and ML algorithms to address the complex, multivariable nature of MAP systems, demonstrating their strong potential for accurately predicting product yields and process parameters (Chen et al., 2024; Jiang et al., 2024; Liu et al., 2024b; Narde & Remya, 2022; Palla et al., 2024; Ren et al., 2022; Shen et al., 2022; Yang et al., 2022; Zhong et al., 2024). Table 1 presents a summary of prior works and the novelty of the present study. They have shown that models such as

Table 1
Summary of prior works and novelty of the present study.

Reference	Focus/Contribution	Methodological Scope	Limitation	Novelty of Present Work
Yang et al. (Yang et al., 2022)	ML prediction of biochar, bio-oil, and syngas yields from MAP	Predictive modeling (temperature, microwave power)	Limited to product prediction, no optimization/decision support	Integrates predictive modeling with optimization and MCDM
Shen et al. (Shen et al., 2022)	Gradient boosting & bagging for multi-output pyrolysis predictions	ML for multiple biomass types	Prediction only; lacks optimization framework	Combined ML + MOGWO + WTM decision-making
Chen et al. (Chen et al., 2024)	LLM + ANN hybrid for sawdust MAP	Hybrid ML for prediction	Focused on single feedstock, no multi-objective optimization	Expanded hybrid framework across modeling, optimization, and decision support
Ren et al. (Ren et al., 2022)	ML + metaheuristic for catalytic and heating efficiency	Separate prediction + optimization	Optimization not linked to systematic decision-making	Integration with MCDM ensures practical scenario-based guidance
Zhong et al. (Zhong et al., 2024)	ANN, SVM, RF comparison for pyrolysis kinetics/ thermodynamics	Model comparison	Focused on interpretability, not multi-objective trade-offs	Surrogate modeling embedded in optimization loop
Liu et al. (Liu et al., 2024b)	Mechanistic ML insights on biomass component interactions	Intrinsic modeling	Did not integrate optimization or scenario ranking	Unified model linking kinetics → optimization → decisions
Jiang et al. (Jiang et al., 2024)	AI-driven catalyst selection and reaction efficiency	Optimization focus	Not generalized to broader MAP framework	Broadened scope with holistic, multi-criteria approach
Present study	Hybrid AI-driven framework for PKS MAP	COMBI surrogate modeling + MOGWO optimization + WTM decision-making	–	First comprehensive integration of ML, metaheuristic optimization, and MCDM for MAP; scalable and structured for real-world application

ANNs, SVMs, RFs, and GPRs can reliably capture nonlinear relationships, while AI algorithms and metaheuristic optimization have been explored separately for improving energy efficiency, catalytic performance, or yield distribution. These contributions highlight the importance of intelligent computing but remain largely fragmented, focusing on either predictive modeling or optimization in isolation. What is still lacking is a comprehensive framework that holistically integrates robust ML surrogate modeling with multi-objective metaheuristic optimization and systematic multi-criteria decision-making (MCDM). To bridge this gap, the present study proposes an innovative hybrid strategy designed to model, optimize, and guide decision-making for MAP systems in a structured and scalable manner.

This research unfolds through a four-phase approach: (1) input-output correlation and data exploration, (2) predictive modeling using the COMBI algorithm, (3) simultaneous multi-objective optimization via the multi-objective grey wolf optimizer (MOGWO), and (4) prioritization and selection of optimal operating scenarios using the weighted Tchebycheff method (WTM). In the modeling stage, the COMBI algorithm is utilized to establish accurate surrogate models for predicting key pyrolysis responses (calorific value, fixed carbon content, and volatile matter content) as functions of critical process variables such as reaction time, sample mass, and nitrogen gas flow rate. To refine process performance, the surrogate models are embedded within the MOGWO algorithm to generate Pareto-optimal trade-offs across competing thermal objectives. The resulting Pareto front is then evaluated using the WTM decision-making framework to rank and select representative design solutions based on varying objective priorities aligned with practical scenarios. By seamlessly integrating advanced surrogate modeling, metaheuristic optimization, and MCDM, this research effectively addresses a notable methodological shortfall and provides a robust framework for enhancing both the effectiveness and overall value of bio-char generation from palm PKS. The schematic flow of this integrated framework is depicted in Fig. 1, highlighting its potential to contribute to sustainable biomass valorization and the broader transition towards cleaner thermal processing technologies.

2. Machine learning modeling

2.1. Data analysis

The data from Jamaluddin et al. (Ismail et al., 2013) were used as a case study for the mixed method presented in this study. Jamaluddin and colleagues aimed to enhance the pyrolysis process of PKS by implementing microwave-assisted pyrolysis, focusing on converting palm oil waste into high-quality bio-char. Their research sought to identify the ideal operational conditions that would yield bio-char with superior calorific value and fixed carbon content while keeping the volatile matter content low and maximizing the overall yield. This approach addressed the inefficiencies of traditional biomass combustion methods and showcased microwave radiation-induced pyrolysis as a more sustainable and energy-efficient alternative for transforming agricultural waste into valuable products. In their work, Jamaluddin et al. adopted response surface methodology (RSM) combined with a central composite rotatable design (CCRD) to systematically investigate the effects of key operational parameters on the pyrolysis process. Their method involved conducting experimental tests, carefully designed to cover factorial, axial, and central points that maximized the information gained with a limited number of runs. The experiments varied three principal factors (reaction time (RT: 15–45 min), sample mass (SM: 10–30 g), and nitrogen gas flow rate (NGR: 100–300 mL/min)) to study their influence on the performance indicators of the pyrolysis system. The researchers developed regression models that captured the interactions among variables, assessed the significance of each factor, and determined the best operational conditions for producing high-quality bio-char. The study focused on three main output parameters: calorific value (CV), fixed carbon content (FCC), and volatile matter content (VMC). The target was to maximize both the calorific value and the fixed carbon content while keeping the volatile matter as low as possible. Their findings showed that increasing the reaction time generally enhanced the calorific value and fixed carbon content, while slightly lowering the yield due to better removal of volatile components. The results highlighted the feasibility of producing high-quality bio-char with favorable energy properties and emphasized the practical advantages of microwave pyrolysis over conventional methods, particularly in terms of efficiency, product quality, and sustainable waste management. A detailed schematic diagram of the microwave-assisted pyrolysis system employed for converting palm kernel shell into bio-char under controlled conditions is presented in Fig. 2, illustrating the main components and operational setup used throughout the experimental procedure.

Table 2 presents the descriptive statistics of the input and output variables used in the analysis. Among the input variables, reaction time ranged from 4.77 to 55.23 min with a mean and median of 30 min, showing a standard deviation of 12.718 and a variance of 161.74,

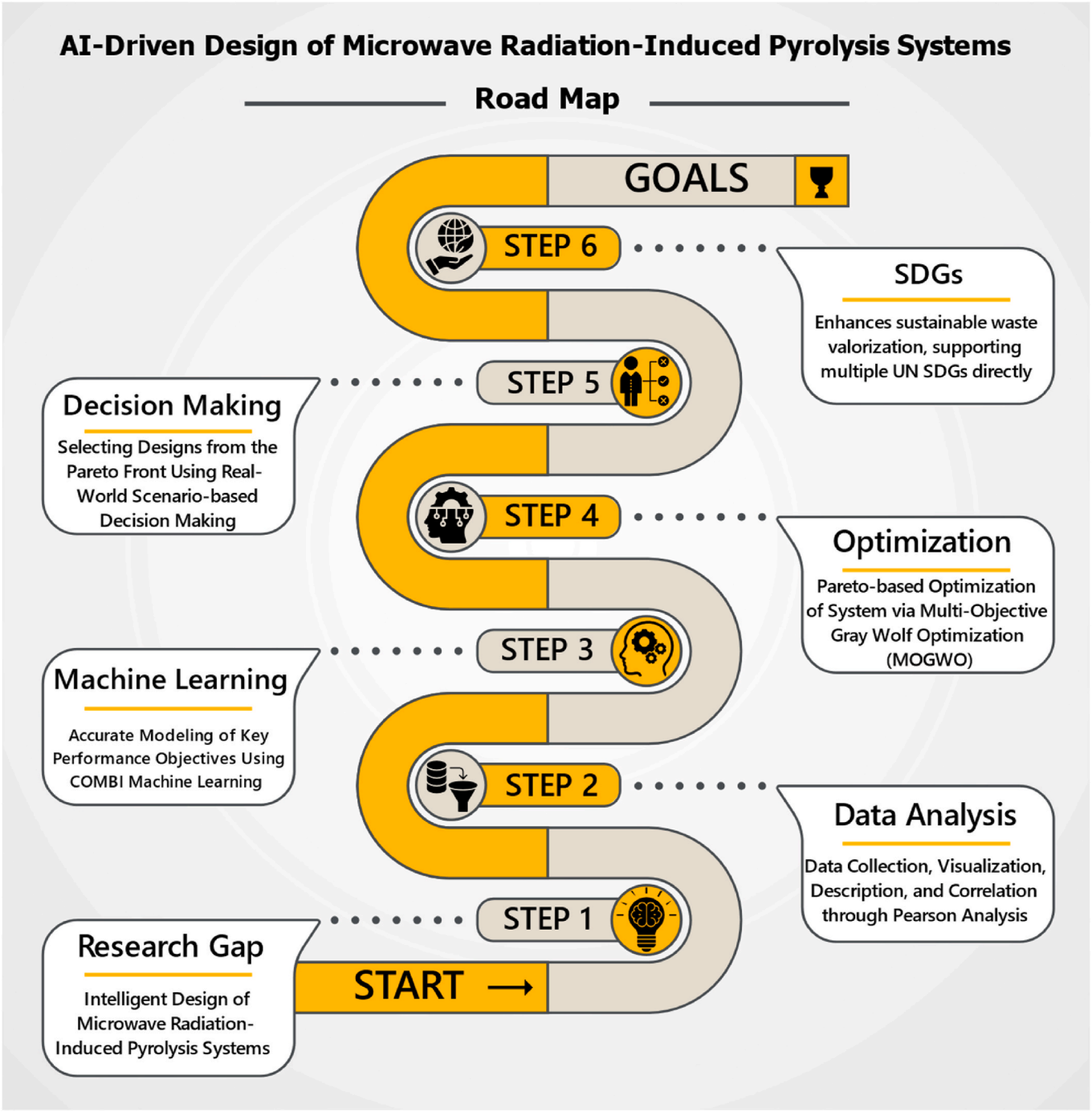

Fig. 1. Schematic flow of the proposed AI-based framework for microwave pyrolysis of palm kernel shells, integrating data analysis, COMBI surrogate modeling, MOGWO multi-objective optimization, and WTM-based solution ranking.

indicating moderate dispersion. Its coefficient of variation (0.424) reflects this spread relative to the mean. Similarly, sample mass varied between 3.18 and 36.82 g, also centered at a mean and median of 20 g, with a standard deviation of 8.479 and variance of 71.89, highlighting comparable variability (CV = 0.424). The nitrogen gas flow rate spanned from 31.82 to 368.18 mL/min, again averaging 200 mL/min with the same coefficient of variation (0.424), a standard deviation of 84.781, and a higher variance of 7187.8, which reflects a broader absolute range. Regarding the output variables, the calorific value ranged between 17 and 30.9 MJ/kg, with a mean of 26.97 MJ/kg and a median of 28.65 MJ/kg. Its variance (10.89) and standard deviation (3.299) were lower than those of FCC and VMC, resulting in a relatively low coefficient of variation (0.122). The FCC ranged from 20.08 to 64.5 wt %, with a mean of 52.114 wt% and a median of 56.125 wt%, displaying a variance of 136.83 and a standard deviation of 11.697, giving a moderate coefficient of variation of 0.224. In contrast, the VMC had a range of 32.94–78.1 wt%, a mean of 45.204 wt%, and a median of 39.485 wt%, accompanied by a variance of 145.93 and a standard deviation of 12.080, yielding a coefficient of variation of 0.267. Skewness and kurtosis results indicate that all three inputs had neutral skewness and slightly platykurtic distributions (kurtosis ≈ -0.183), while among outputs, CV and FCC were negatively skewed (-1.749 and -1.475 respectively) and moderately leptokurtic (kurtosis 3.282 and 1.741), suggesting longer left tails, whereas VMC showed positive skewness

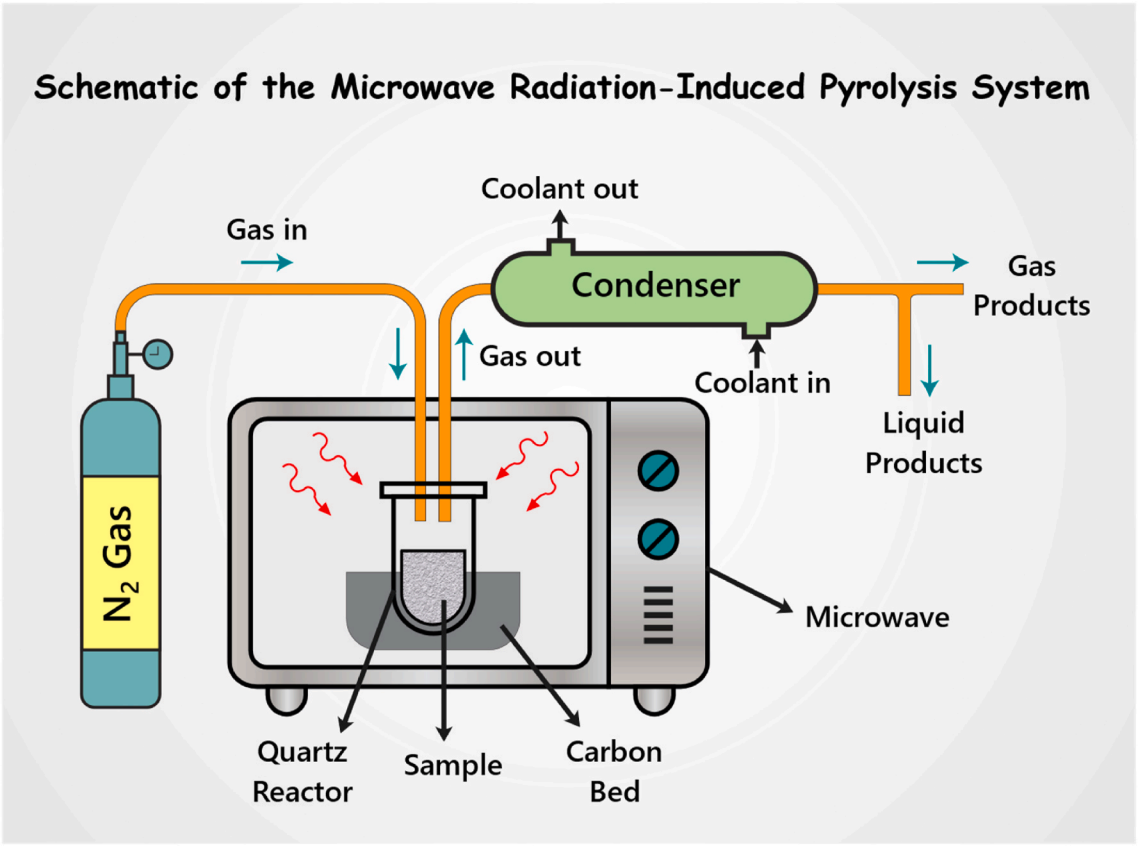

Fig. 2. Diagrammatic illustration of the radiation-assisted pyrolysis setup applied for optimizing the conversion of palm kernel shell.

Table 2
Descriptive statistics of input variables (reaction time, sample mass, nitrogen gas flow rate) and output responses (calorific value, fixed carbon content, volatile matter content), showing the most important statistical characteristics to summarize the dataset used in the hybrid framework.

Statistical Parameters	Input			Target		
	RT (min)	SM (g)	NGFR (mL/min)	CV (MJ/kg)	FCC (wt%)	VMC (wt%)
Minimum	4.77	3.18	31.82	17	20.08	32.94
Maximum	55.23	36.82	368.18	30.9	64.5	78.1
Mean	30	20	200	26.97	52.114	45.204
Median	30	20	200	28.65	56.125	39.485
Variance	161.74	71.89	7187.8	10.89	136.83	145.93
Standard deviation	12.718	8.479	84.781	3.299	11.697	12.080
Coefficient of variation	0.424	0.424	0.424	0.122	0.224	0.267
Skew	0	0	0	−1.749	−1.475	1.546
Kurtosis	−0.183	−0.183	−0.183	3.282	1.741	1.724
Kolmogorov-Smirnov stat	0.25	0.25	0.25	0.261	0.258	0.32

(1.546) and kurtosis of 1.724, reflecting a longer right tail and a relatively peaked distribution. Finally, the Kolmogorov-Smirnov statistics ranged from 0.25 to 0.32 across all variables, pointing to mild deviations from normality in data distribution. The descriptive statistics presented provide clear insight into the distribution and variability of the output variables, which is essential for understanding how the pyrolysis system behaves under different conditions. By showing the range, mean, variance, standard deviation, and coefficients of variation for calorific value, fixed carbon content, and volatile matter content, the data reveal how consistently these outputs perform and how they are spread around their means. The skewness and kurtosis further clarify the shape of each output's distribution, highlighting any tendencies toward outliers or asymmetry. Together, these statistics ensure that the input–output relationships are well-characterized, offering a stable and reliable foundation for developing robust models and effective optimization strategies in this study.

Fig. 3 presents a comprehensive visualization of the distribution characteristics of the three key output variables, which are statistically summarized in Table 2. As observed in Fig. 3(a), the CV distribution is left-skewed (Skew = −1.749), with a peak frequency between 29 and 32 MJ/kg, aligning with the highest frequency class (40 %). This reflects the concentration of values near the upper end of the range, corroborated by the high kurtosis (3.282), indicating a leptokurtic distribution. Fig. 3(b) confirms this pattern, with the median (28.65 MJ/kg) close to the upper quartile, as also seen in Table 2. Similarly, FCC data in Fig. 3 (c) exhibit mild negative skewness (−1.475), with the highest frequency occurring at 50–60 wt%, aligning well with the median (56.13 wt%) and mean (52.11 wt%) reported in the table. Fig. 3(d) further supports this with a moderately concentrated distribution and a slight extension towards lower values, consistent with the histogram. In contrast, VMC values shown in Fig. 3(e) are positively skewed (1.546), indicating a concentration of data points towards lower values (30–40 wt%), with a

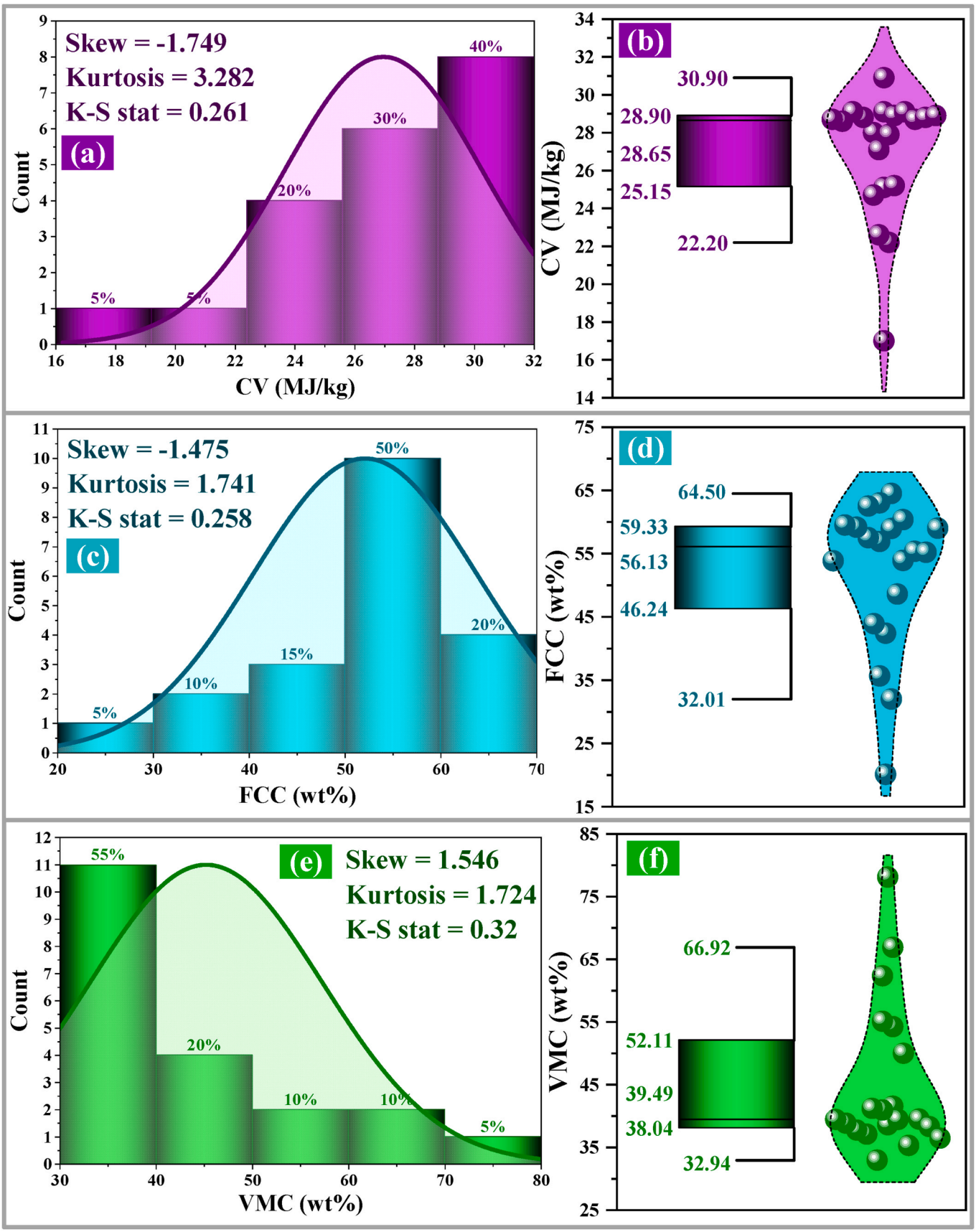

Fig. 3. Histogram and box/violin plots showing the distribution of key pyrolysis outputs (calorific value (CV), fixed carbon content (FCC), and volatile matter content (VMC)) highlighting data spread, central tendency, and variability to inform surrogate modeling and optimization.

long tail extending toward higher contents. The histogram reveals that over 55 % of samples fall within the lowest bin, and the box plot in in Fig. 3(f) confirms this skew, showing a median of 39.49 wt% significantly lower than the mean of 45.20 wt%. The Kolmogorov-Smirnov statistics for all three outputs suggest moderate deviations from normality, particularly for VMC (K-S = 0.32), supporting the use of nonlinear modeling.

The Pearson correlation coefficient (PCC) is a widely used statistical metric that quantifies the strength and direction of the linear relationship between two continuous variables (Sedgwick, 2012). Mathematically, it is calculated as the covariance of the two variables divided by the product of their standard deviations (Alsehli et al., 2024):

$$PCC = \frac{\sum_{i=1}^{N}(X_i - \overline{X})(Y_i - \overline{Y})}{\sqrt{\sum_{i=1}^{N}(X_i - \overline{X})^2 \sum_{i=1}^{N}(Y_i - \overline{Y})^2}} \quad (1)$$

In this formula, X_i and Y_i represent each individual observation, while $\overline{X}$ *and* $\overline{Y}$ denote their average values. The resulting coefficient can vary from −1 to +1, where values near the extremes signify a strong negative or positive linear connection, and values near zero indicate little to no linear dependency between the variables.

Fig. 4 illustrates the Pearson correlation coefficients quantifying the linear relationships among the key process variables and the primary target outputs. This matrix provides initial insight into how each operational factor can affect the thermal performance and quality of the produced bio-char. Notably, RT demonstrates a strong positive correlation with CV and FCC, at 0.76 and 0.84 respectively, implying that extending reaction time significantly enhances both the calorific value and fixed carbon proportion in the char product. Meanwhile, RT shows a strong negative correlation with VMC at −0.83, highlighting its effectiveness in reducing volatile matter through prolonged thermal decomposition. The correlation of SM with the outputs is relatively weak, with coefficients of 0.14 for CV, 0.13 for FCC, and −0.12 for VMC, suggesting that within the tested range, sample mass exerts only a mild linear impact on output quality. Similarly, NGFR's direct linear effect appears negligible with correlations of −0.12 with CV, −0.03 with FCC, and a slightly positive 0.08 with VMC, indicating that its influence may be more nuanced or nonlinear in nature. The outputs themselves exhibit very high correlations: CV and FCC are almost perfectly correlated (0.96), which makes sense since higher calorific value typically coincides with higher fixed carbon content. Both outputs show a near-perfect inverse correlation with VMC (−0.98 for CV and −0.99 for FCC), reflecting the inherent trade-off, where improving energy density and carbon fraction directly reduces undesirable volatiles. It is critical to emphasize that the low correlations should not be overlooked; these values only reflect linear trends and do not capture hidden nonlinear interactions that could significantly influence process behavior. This underlines the value of advanced machine learning modeling like the COMBI algorithm used in this study, which can reveal complex dependencies that simple correlation analysis cannot detect.

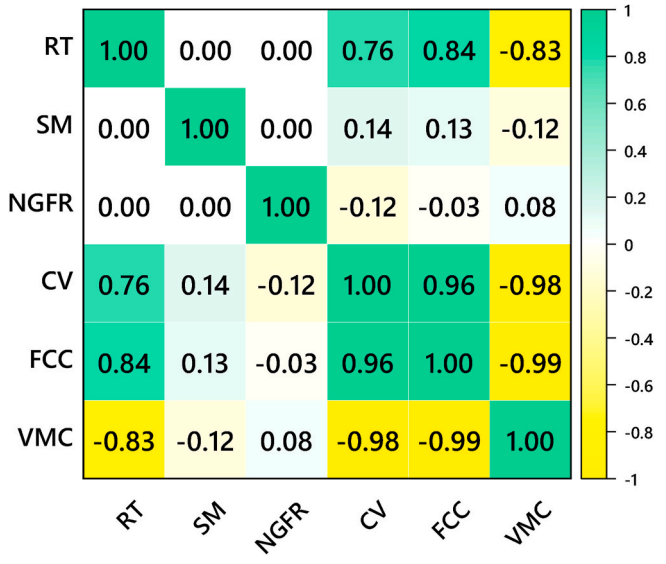

Fig. 4. Pearson correlation matrix illustrating the linear relationships among process inputs and target outputs for microwave-assisted pyrolysis of PKS.

2.2. Combinatorial algorithm

The COMBI algorithm, which forms a core element of the group method of data handling (GMDH), is developed to capture intricate system behaviors by determining the best-fitting polynomial functions from the available data (Koshulko et al., 2014, p. 81). The procedure starts with organizing the input data into a matrix format, comprising N samples described by M variables. This data matrix is then split into two parts: one designated for training (N_A) and the other for validation (N_B). The training portion is employed to calculate the coefficients of potential polynomial models, whereas the validation portion is used to assess the quality of these models based on a regularity measure, commonly the average regularity (AR) criterion, which is mathematically formulated as follows:

$$AR(s) = \frac{1}{N_B}\sum_{i=1}^{N_B}(y_i - \hat{y}_i)^2 \rightarrow min \quad (2)$$

where y_i denotes the actual output and $\hat{y}_i$ is the predicted output. Alternatively, the algorithm may adopt the Predictive Residual Sum of Squares (PRESS) metric, which uses cross-validation techniques to make full use of the entire dataset. The PRESS criterion is defined as the mean of the squared differences between observed and predicted values, mathematically represented as:

$$PRESS(s) = \frac{1}{N}\sum_{i=1}^{N}(y_i - \hat{y}_i)^2 \rightarrow min \quad (3)$$

This approach aims to minimize the predictive error, thereby enhancing model generalization. In essence, Eq. (3) applies a cross-validation approach where the dataset is partitioned so that each observation serves once as the validation point, equivalent to performing leave-one-out cross-validation. Although this strategy demands substantial computational resources, its precision justifies its use as a validation tool in the present work. The COMBI procedure systematically explores possible models, categorizing them according to their structural complexity. At the first stage, it evaluates simple models involving single predictor variables:

$$y = a_0 + a_1 x_i, i = 1, 2, \ldots, M \quad (4)$$

In the following stages, it expands this search to models that combine two predictor variables:

$$y = a_0 + a_1 x_i, + a_2 x_j, i = 1, 2, \ldots, M \quad (5)$$

During each iteration, the algorithm assesses the candidate models using the specified evaluation metric and proceeds iteratively until it locates the configuration that achieves the lowest metric value, signifying the most accurate model. To reduce computational demands, it can narrow down the search space by retaining only the top-ranked variables at an intermediate stage, allowing the detailed search in the following layers to concentrate on this refined subset of promising predictors.

In this study, additional terms were incorporated into the fundamental polynomial structure to enrich the diversity and intricacy of relationships between the independent and dependent variables. This

approach is illustrated through the following example (Hai et al., 2025):

$$y = \sum_{i=1}^{n} \beta_i g(x_i) \tag{6}$$

$$y = \sum_{i=1}^{n} \sum_{j=1}^{n} \beta_{ij} g(x_i) \cdot g(x_j) \tag{7}$$

$$y = \sum_{i=1}^{n} \sum_{j=1}^{n} \beta_{ij} g(x_i) \,/\, g(x_j) \tag{8}$$

The function $g(x)$ applies an extended collection of operators to transform the input features, thereby improving how they are represented and contributing to greater modeling precision. This broader operator set (covering functions such as trigonometric transformations, sigmoid, powers (square and cubic), roots (square root and cube root), exponential terms, and additional forms) enables the model to capture more complex relationships with the response variables. Furthermore, the parameters within the model are estimated during training by employing the least squares method to ensure the best possible fit.

The computational intensity associated with the COMBI algorithm affects its overall efficiency, necessitating a careful balance between predictive accuracy and structural complexity. Although less complex models often yield lower precision, ensuring the practical feasibility of the resulting models demands the application of strict constraints on their complexity to prevent overfitting and maintain interpretability. This method has demonstrated high efficiency in regression modeling across various fields, particularly with small datasets (Abdollahi et al., 2024a; Sepehrnia et al., 2022; Zhang et al., 2024).

2.3. Model development and evaluation

The modeling strategy employs a whole search technique (WST) designed to refine both the structural design and hyperparameter settings of machine learning models. This approach has proven effective for accurately tuning machine learning algorithms, as shown in prior research (Sepehrnia et al., 2025; Zhang et al., 2023). Within the COMBI context, this technique focuses on selecting the most effective operators and functions to process the input variables accurately. Moreover, WST systematically adjusts the number of additional sub-models, maintaining an appropriate level of model complexity and computational efficiency (Abdollahi et al., 2024b). Also, WST identifies the most appropriate set of operators and functional transformations to apply to the input data, further enhancing the model's predictive capability. Based on the WST performance, striking an optimal balance between simplicity and predictive reliability is crucial when constructing models. This balance is achieved by deliberately limiting the model's complexity, primarily by capping the total number of terms included. Through iterative experimentation and a series of trial-and-error tests, the machine learning framework in this study was restricted to a maximum of ten terms (sub-models). Imposing such constraints helps produce models that remain computationally efficient and practically applicable, ensuring they are robust enough for real-world implementation while avoiding unnecessary overfitting. In addition, convergence analysis showed that accuracy improvements beyond ten sub-models were marginal, while model complexity and computational cost increased significantly. Furthermore, similar limitations on the number of sub-models have been reported in previous studies such as Hai et al. (Hai et al., 2025), Sepehrnia et al. (Sepehrnia et al., 2022), and Zhang et al. (Zhang et al., 2024), which confirms the validity of this design choice.

In addition, the available data were divided such that 80 % served for model training and the remaining 20 % were reserved exclusively for performance testing. The evaluation of the machine learning models' predictive capability is carried out using five distinct statistical indicators (Eqs. (9)–(13)) (Basem et al., 2024; Hai et al., 2024a, 2024b).

These performance measures incorporate the variables $Y_{i,Act}$ and $Y_{i,Pred}$, denoting the actual results and the corresponding model predictions, respectively, along with n, which indicates the total sample size considered in the analysis.

$$\text{Mean squared error}: MSE = \frac{1}{n} \sum_{i=1}^{n} \left(Y_{i,Act} - Y_{i,Pred}\right)^2 \tag{9}$$

$$\text{Mean absolute percentage error}: MAPE(\%) = \frac{1}{n} \sum_{i=1}^{n} \left| \frac{Y_{i,Pred} - Y_{i,Act}}{Y_{i,Act}} \right| \times 100 \tag{10}$$

$$\text{Correlation coefficient}: R = \frac{\sum_{i=1}^{n} \left(Y_{i,Act} - \overline{Y_{i,Act}}\right)\left(Y_{i,Pred} - \overline{Y_{i,Pred}}\right)}{\sqrt{\sum_{i=1}^{n} \left(Y_{i,Act} - \overline{Y_{i,Act}}\right)^2 \sum_{i=1}^{n} \left(Y_{i,Pred} - \overline{Y_{i,Pred}}\right)^2}} \tag{11}$$

$$\text{Coefficient of determination}: R^2 = 1 - \sum_{i=1}^{n} \frac{\left(Y_{i,Pred} - Y_{i,Act}\right)^2}{Y_{i,Act}^2} \tag{12}$$

$$\text{Willmott's Index of Agreement}: I_A = 1 - \frac{\sum_{i=1}^{n} \left(Y_{i,Act} - Y_{i,Pred}\right)^2}{\sum_{i=1}^{n} \left(\left|Y_{i,Pred} - \overline{Y_{i,Act}}\right| + \left|Y_{i,Act} - \overline{Y_{i,Act}}\right|\right)^2} \tag{13}$$

The model's predictive accuracy is evaluated using MAPE and MSE, which measure the magnitude of prediction errors. Conversely, the R, R^2, and I_A assess the level of agreement between the actual observations and the model's predictions. These agreement metrics vary between 0 and 1, where values closer to 1 signify a higher degree of consistency and superior model performance.

2.4. Modeling results

Table 3 presents a comprehensive evaluation of the COMBI model's performance across three objectives (CV, FCC, and VMC) for both training and testing datasets using multiple statistical criteria. For the calorific value, the testing dataset demonstrates exceptional accuracy, with a very low MSE of 0.118 and MAPE of just 1.002 %, indicating minimal deviation between predicted and actual values. The correlation coefficient of 0.9993 and R^2 of 0.9986 confirm a near-perfect linear relationship, while the index of agreement of 0.9983 further supports strong concordance. The training results for CV are similarly robust, showing an MSE of 0.079 and MAPE of 0.836 %, with slightly lower but still impressive R (0.9932), R^2 (0.9865), and I_A (0.9964), reflecting reliable model generalization without overfitting. Regarding fixed carbon content, the testing dataset also exhibits strong predictive capability, with an MSE of 0.314 and MAPE of 1.285 %. The high R (0.9993), R^2 (0.9985), and I_A (0.9996) values indicate excellent agreement and precision in estimating FCC. However, the training dataset for FCC

Table 3
Performance evaluation of the COMBI model for predicting calorific value, fixed carbon content, and volatile matter content across training and testing datasets using key statistical metrics.

Objective	Dataset	MSE	MAPE (%)	R	R^2	I_A
CV	Testing	0.118	1.002	0.9993	0.9986	0.9983
	Training	0.079	0.836	0.9932	0.9865	0.9964
FCC	Testing	0.314	1.285	0.9993	0.9985	0.9996
	Training	2.249	2.254	0.9865	0.9732	0.9931
VMC	Testing	1.478	2.620	0.9984	0.9967	0.9978
	Training	1.397	2.228	0.9949	0.9898	0.9972

shows comparatively higher error metrics, with an MSE of 2.249 and MAPE of 2.254 %, alongside slightly lower correlation coefficients (R = 0.9865, R^2 = 0.9732) and I_A of 0.9931. This suggests that while the model fits well, the variability in training data may be higher or more complex, leading to increased prediction error during training but strong performance on unseen data. For volatile matter content, the testing set reveals an MSE of 1.478 and MAPE of 2.620 %, indicating moderate prediction errors relative to the other objectives. Still, the statistical indicators remain high, with R = 0.9984, R^2 = 0.9967, and I_A = 0.9978, highlighting a very good match between predicted and actual values. Training performance for VMC is consistent with testing results, showing an MSE of 1.397 and MAPE of 2.228 %, and slightly higher R (0.9949), R^2 (0.9898), and I_A (0.9972) values, which reflect stable and reliable model fitting.

For comparison, Jamaluddin et al. (Ismail et al., 2013) developed models using response surface methodology. While their approach is widely used, it achieved lower predictive accuracy, with R^2 values of 0.9657 for CV, 0.9495 for FCC, and 0.9640 for VMC. In contrast, the COMBI model provides substantially higher accuracy (R^2 > 0.996 for testing datasets), capturing more complex multivariate interactions and demonstrating superior reliability in predictions. Therefore, these statistics and comparison illustrate that the COMBI model delivers highly accurate and consistent predictions across all objectives, with particularly strong performance on the testing datasets, indicating robust generalization capabilities. The low error rates and high agreement measures suggest that the model effectively captures the underlying relationships in the data, making it a powerful tool for estimating critical parameters in the pyrolysis process.

Fig. 5 combines violin plots and box plots to illustrate the predictive performance of the optimized COMBI models for CV, FCC, and VMC for both actual and predicted data points. For the CV (Fig. 5(a)), the distribution of actual values spans from approximately 25.15 to 28.90 MJ/kg, while the predicted data range closely aligns, from about 25.31 to 28.90 MJ/kg. The violin shapes show that the predicted data distribution mirrors the actual data's density peaks, indicating the model's capacity to capture the variation patterns reliably. The box plots embedded within the violins confirm that the median and interquartile ranges of the predicted and actual CV data are almost identical, reflecting negligible deviation and demonstrating high prediction precision. In Fig. 5(b), for FCC, the actual data ranges from roughly 46.24

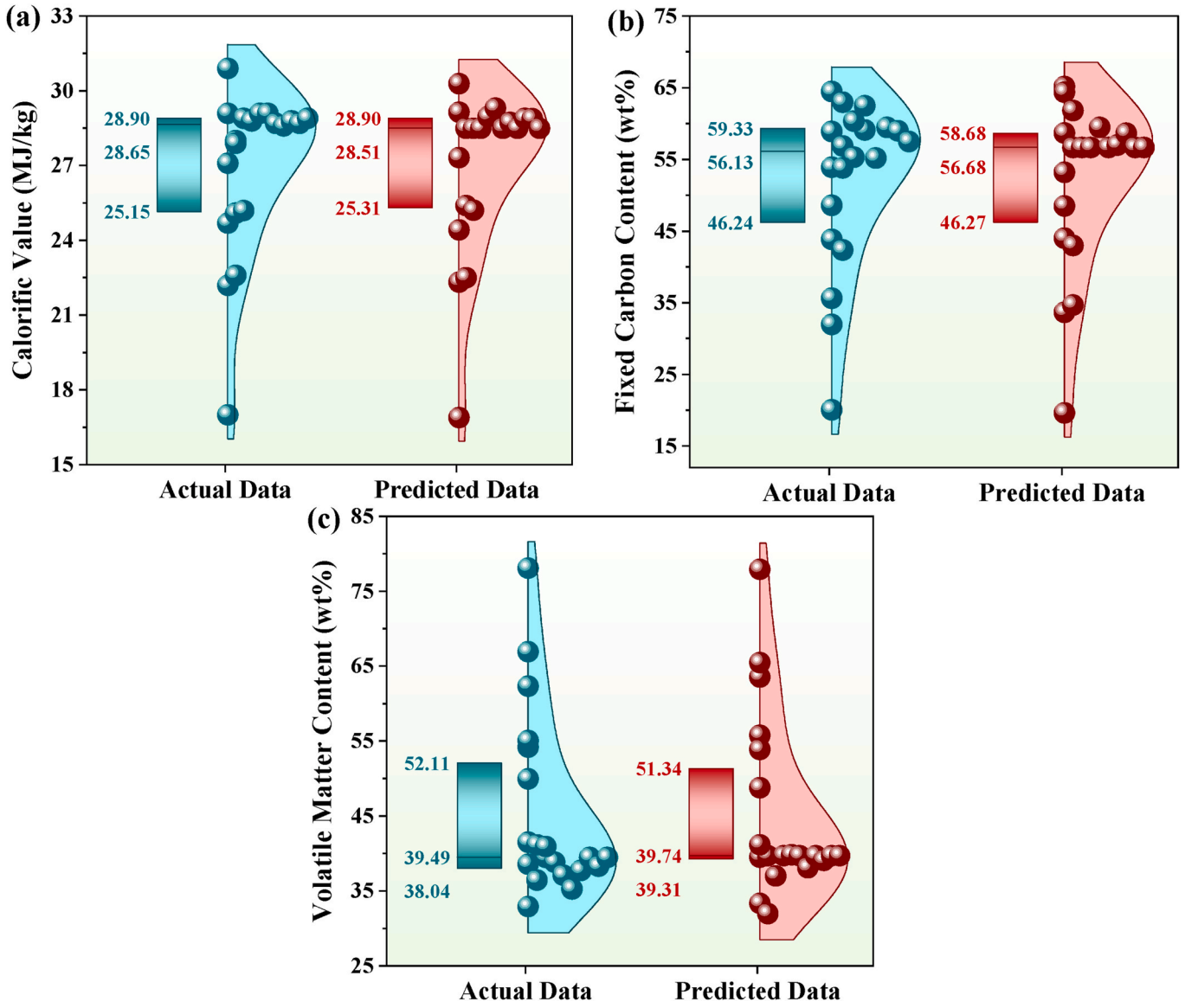

Fig. 5. Combined violin and box plots comparing actual and COMBI-predicted values of (a) calorific value, (b) fixed carbon content, and (c) volatile matter content, illustrating prediction accuracy, distribution overlap, and variability for model validation.

%–59.33 % wt, with predicted values slightly lower at 46.27 %–58.68 % wt. The violin plots for FCC reveal a similarly tight alignment, with both predicted and actual data showing comparable density bulges around 56 % wt. The box plots again support this consistency, with overlapping medians and quartiles highlighting that the COMBI model captures the central tendency and spread of FCC accurately. In Fig. 5(c), the VMC results show a strong match as well: actual values spread from about 38.04 % to 52.11 % wt, while predicted values span from 39.31 % to 51.34 % wt. Although slight variations appear at the tails, the overall shapes of the violins indicate that the model effectively replicates the true distribution, especially within the core range. The box plots emphasize this, with the predicted VMC median and quartiles closely following the actual data, confirming minimal bias. This robust predictive accuracy offers a solid foundation for subsequent multi-objective optimization, ensuring that decision-making and trade-off analyses rest on dependable surrogate models that faithfully represent the complex thermal behavior of the process.

Fig. 6 presents the sensitivity analysis of key input parameters on the three main performance indicators of the pyrolysis process. Fig. 6(a) and (b) illustrate how CV responds to variations in RT, SM, and NGFR using the optimized COMBI model. In Fig. 6(a), where NGFR is held constant at 200 mL/min, increasing RT consistently enhances CV, particularly when SM is above 14 g. The optimal region for achieving maximum CV is observed between RT = 35–45 min and SM = 18–30 g, where CV values reach or exceed 29 MJ/kg. Conversely, when SM falls below 14 g, the increase in CV becomes less effective. Fig. 6(b) shows that at a fixed SM of 20 g, CV rises with RT, reaching a peak above 30 MJ/kg at RT = 30–45 min and NGFR = 100–140 mL/min. However, as NGFR increases, the enhancement diminishes, likely due to reduced thermal efficiency caused by excess gas flow. Fig. 6(c) and (d) reveal similar trends for FCC. With NGFR fixed at 200 mL/min in Fig. 6(c), FCC remains below 50 wt% for RT < 25 min but increases sharply beyond 30 min, peaking at ~63.5 wt% when SM is within 16–30 g. Notably, SM below 14 g fails to support high FCC development. Fig. 6(d), at a fixed SM of 20 g, demonstrates that optimal FCC values above 63 wt% occur at RT = 35–45 min and NGFR = 100–160 mL/min, while higher NGFR levels (>240 mL/min) reduce FCC due to possible heat loss or insufficient reaction time. Finally, Fig. 6(e) and (f) display the response of VMC to the same input variables. Fig. 6(e), with NGFR fixed at 200 mL/min, shows a sharp decline in VMC—from above 65 wt% at RT = 15 min to below 38 wt% beyond RT = 30 min. The lowest VMC (~32.35 wt%) occurs when RT exceeds 40 min and SM is in the 16–30 g range. Similarly, Fig. 6(f), at SM = 20 g, confirms that VMC decreases with RT and reaches a minimum (~32.82 wt%) at RT = 43 min and NGFR = 100–160 mL/min. However, NGFR above 240 mL/min leads to elevated VMC, likely due to thermal dilution or premature volatile removal. Overall, these results consistently identify RT as the dominant parameter for optimizing CV and FCC while minimizing VMC, with SM and NGFR serving as secondary but critical modulators for tuning the pyrolysis system.

3. Multi-objective optimization

In complex engineering and energy systems such as the one examined in this study, multiple conflicting objectives often need to be addressed simultaneously, making multi-objective optimization (MOO) an essential component of the design and decision-making process. Unlike conventional single-objective methods that yield a single optimal point, MOO recognizes the trade-offs among competing goals and provides a diverse set of equally optimal solutions known as the Pareto front. This Pareto-based perspective enables decision-makers to balance priorities more effectively, considering both technical performance and practical constraints. To achieve this, various evolutionary and swarm-based meta-heuristic algorithms are commonly employed due to their robustness in navigating complex, multi-dimensional search spaces. Mathematically, the present MOO problem can be expressed as:

$$\begin{cases} Maximize\ CV = f(RT, SM, NGFR) \\ Maximize\ FCC = g(RT, SM, NGFR) \\ Minimize\ VMC = h(RT, SM, NGFR) \\ Subject\ to \begin{cases} 4.77 \le RT \le 55.23\ (min) \\ 3.18 \le SM \le 36.82\ (g) \\ 31.82 \le NGFR \le 368.18\ (mL/min) \end{cases} \end{cases} \tag{14}$$

Eq. (14) describes the multi-objective framework using surrogate functions *f*, *g*, and *h*, each representing a predictive model developed through the COMBI algorithm.

3.1. Multi-objective grey wolf optimizer

The multi-objective grey wolf optimizer is an enhanced version of the original grey wolf optimizer (GWO), developed to solve multi-objective problems by emulating the social hierarchy and cooperative hunting behavior of grey wolves (Mirjalili et al., 2016). In the original GWO framework, candidate solutions are organized in a pack structure where the top three solutions assume the leadership roles: alpha (α), beta (β), and delta (δ). These leading agents guide the remaining wolves, known as omega (ω), directing them toward the most promising regions of the search space. This leader-follower structure ensures a dynamic balance between exploration of the solution landscape and exploitation of the best-found regions (Mirjalili et al., 2014).

In MOGWO, this principle is adapted to handle multiple conflicting objectives by introducing two vital mechanisms: an external archive that stores the set of non-dominated solutions and a strategy to select diverse leaders from this archive (Faris et al., 2018). The position update mechanism, which models the wolves' encircling behavior, uses the following fundamental equations:

$$\vec{D} = \left| \vec{C} \cdot \vec{X}_p(t) - \vec{X}(t) \right| \tag{15}$$

$$\vec{X}(t+1) = \vec{X}_p(t) - \vec{A} \cdot \vec{D} \tag{16}$$

Here, $\vec{X}_p(t)$ represents the estimated prey position (guiding solution), $\vec{X}(t)$ is the current position of the search agent, and $\vec{A}$ *and* $\vec{C}$ coefficient vectors calculated as:

$$\vec{A} = 2\vec{a} \cdot \vec{r}_1 - \vec{a}, \vec{C} = 2 \cdot \vec{r}_2 \tag{17}$$

The parameter $\vec{a}$ decreases linearly from 2 to 0 over the iterations, which manages the balance between exploration (when $|\vec{A}| > 1|$) and exploitation (when $|\vec{A}| < 1$). $\vec{r}_1$ *and* $\vec{r}_2$ are random vectors with elements in the range of 0 and 1, introducing stochastic behavior into the search.

To mimic the collective hunting process, each agent estimates its next position by averaging the influence of the three best leaders:

$$\vec{X}(t+1) = \frac{\vec{X}_1 + \vec{X}_2 + \vec{X}_3}{3} \tag{18}$$

In the multi-objective extension, MOGWO maintains an external archive to preserve a well-distributed set of Pareto-optimal solutions. New solutions generated during iterations are added only if they are non-dominated. If the archive reaches its storage limit, a density estimation method based on grid segmentation identifies crowded regions. Solutions in highly populated grid cells are more likely to be removed, ensuring that the archive maintains diversity across the Pareto front.

Leader selection for the next iteration uses a roulette-wheel mechanism, drawing alpha, beta, and delta solutions from the least crowded regions of the archive. The probability of choosing leaders from sparse areas ensures the algorithm continuously explores unexplored or

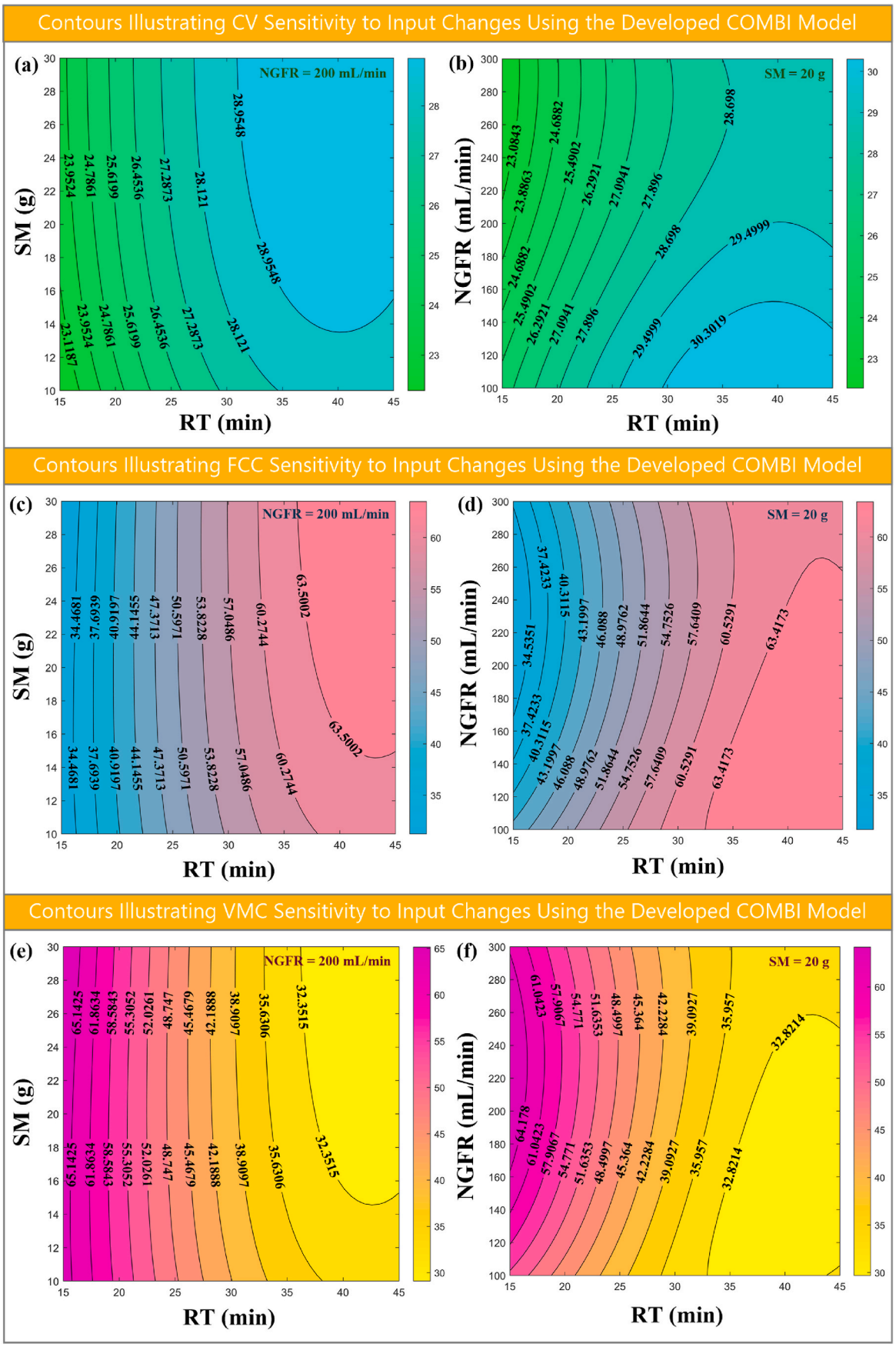

Fig. 6. Sensitivity analysis of CV, FCC, and VMC with respect to the input variables (reaction time, sample mass, and nitrogen gas flow rate) using the optimized COMBI model, highlighting which factors most strongly influence each pyrolysis output.

underrepresented parts of the objective space.

This combination of encircling dynamics, adaptive coefficient control, external archiving, and leader diversity equips MOGWO to transition smoothly between global exploration and local refinement. It retains a computational complexity comparable to leading multi-objective techniques like NSGA-II but achieves improved solution diversity and convergence through its biologically inspired mechanics and robust Pareto management. As a result, MOGWO offers a reliable, efficient, and versatile approach for tackling complex multi-objective optimization tasks in engineering and science (Liu et al., 2024c; Nasir et al., 2024, pp. 1–41).

3.2. Pareto optimal points

Fig. 7 presents the 3D Pareto-optimal solutions obtained using the MOGWO for the microwave-assisted pyrolysis of PKS, with the objective of maximizing calorific value and fixed carbon content, while minimizing volatile matter content. The trade-off relationships among the three target variables are clearly visualized in the figure. As seen, CV and FCC exhibit a positive correlation, forming a curved Pareto front in the CV–FCC plane, indicating that enhancing the energy density of the bio-char (higher CV) generally coincides with higher carbon retention (FCC). Conversely, an inverse relationship is observed between VMC and the other two parameters, particularly FCC, suggesting that lower volatile content is a desirable feature of high-performance bio-char and typically occurs at higher levels of carbonization. The convexity of the solution set indicates a non-linear trade-off surface, especially evident in the VMC dimension, where further reductions in VMC result in diminishing returns in CV and FCC. The spatial clustering of optimal points implies convergence towards a well-defined region of high-quality bio-char production. The visual distribution also highlights the inherent complexity of simultaneously optimizing energy content, carbon stability, and reduced volatility, highlighting the efficacy of MOGWO in navigating multi-objective landscapes within bioenergy system optimization.

Fig. 8 illustrates the distribution of optimal input parameters corresponding to the three objective functions, obtained from the multi-objective optimization. Fig. 8(a) to 8(c) depict the variation of CV as a function of RT, SM, and NGFR, respectively. It is evident that calorific value exhibits a declining trend as each input variable increases. Specifically, in Fig. 8(a), CV decreases from around 31.1 MJ/kg to approximately 30.2 MJ/kg as RT increases from 38 to 44 min. A similar trend is observed in Fig. 8(b)–(c), where increasing SM from 20 to 30 g and NGFR from 100 to 160 mL/min leads to a gradual reduction in CV. This implies that excessively high values of these inputs may cause energy losses or incomplete carbonization, thus reducing the energy density of the produced bio-char. Also, Fig. 8(d) to 8(f) focus on FCC and show a contrasting behavior. As shown in Fig. 8(d), FCC increases progressively with RT, reaching its highest values around 43–44 min. A similar increasing pattern is observed in Fig. 8(e)–(f) with respect to SM and NGFR. This indicates that prolonged exposure to microwave energy and higher input quantities facilitate greater carbon retention in the bio-char. However, this increase in FCC comes at the expense of reduced CV, highlighting a trade-off that must be carefully managed during optimization. Finally, Fig. 8(g) to 8(i) display the changes in VMC with the three inputs. In all cases, VMC demonstrates a clear declining trend with increasing RT, SM, and NGFR, suggesting that longer residence times and higher operational intensities enhance the release of volatiles from the biomass. This behavior supports the conclusion that more intense pyrolysis conditions promote better devolatilization, yielding more thermally stable bio-char with lower VMC values.

A detailed analysis of these Pareto-optimal points reveals that achieving higher CV values (typically in the range of 30.8–31.12 MJ/kg) is predominantly linked to shorter reaction times (38.7–40.5 min), smaller sample masses (21–23 g), and lower NGFRs (close to 100 mL/min). These combinations indicate that maximizing the energy content of the resulting bio-char is favored under milder processing conditions, likely to prevent over-carbonization or excessive thermal degradation of valuable volatiles. In contrast, the scenarios yielding the highest FCC values (up to 67.78 wt%) are generally associated with longer reaction times (42–43.3 min), larger sample masses (29–30 g), and elevated NGFRs ranging from 140 to 155 mL/min. This pattern clearly reflects the role of prolonged residence time and greater process intensity in enhancing thermal decomposition and solid carbon retention.

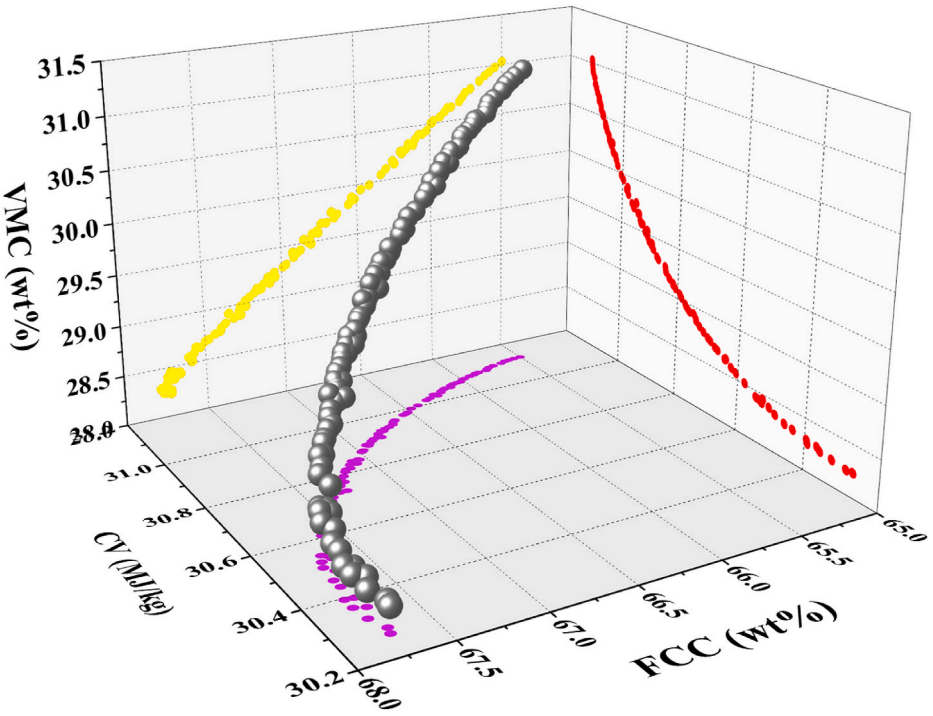

Fig. 7. Three-dimensional Pareto-optimal solutions obtained using the MOGWO algorithm for radiation-assisted pyrolysis of palm kernel shell.

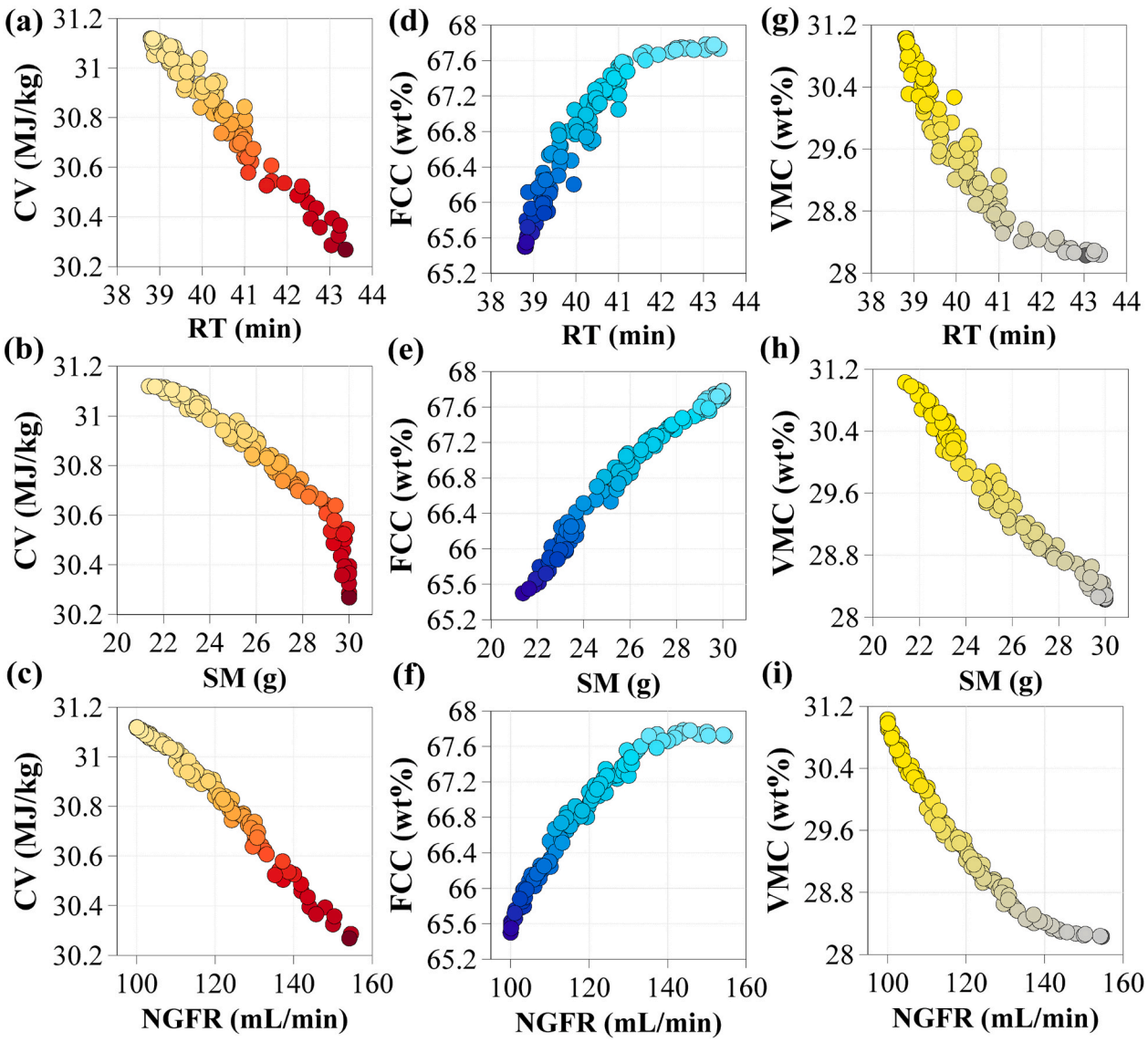

Fig. 8. Influence of input variables on calorific value, fixed carbon content, and volatile matter content at Pareto-optimal points during microwave-assisted pyrolysis of palm kernel shell.

Correspondingly, the lowest VMC values, dropping to about 28.2 wt%, are found under these same high-input conditions, confirming the strong inverse relationship between FCC and VMC. Such findings highlight that more severe pyrolysis conditions promote efficient removal of volatiles while enriching the carbon matrix. However, these benefits come with a slight compromise in CV, which under these settings decreases modestly to around 30.3 MJ/kg. This trade-off illustrates a typical quality-versus-quantity dilemma: while more intense thermal conditions favor structural carbonization and stability (high FCC, low VMC), they may not always coincide with peak energy content (high CV). This multidimensional distribution of input–output combinations emphasizes the necessity for advanced multi-objective optimization strategies, such as the MOGWO algorithm employed in this study, to effectively navigate these competing performance objectives.

A deeper examination of the optimal inputs and their quantitative analysis can uncover significant insights into the system's optimal points. Investigation of the reaction time distribution within the Pareto front reveals a pronounced tendency toward shorter durations. Specifically, 55 % of the optimal data points lie within the lower RT range of 38.79–40.31 min, suggesting that shorter reaction times often present the most favorable compromise between the three target outputs. Meanwhile, 32 % of the solutions occupy the medium RT range of 40.32–41.84 min, indicating that moderate increases in residence time can still produce competitive trade-offs, especially for solutions prioritizing higher carbon content without significantly sacrificing energy yield. In comparison, only 13 % of the solutions fall within the high RT bracket of 41.85–43.37 min, which suggests that while extended pyrolysis may enhance carbon retention, its marginal benefits diminish relative to energy input costs and practical processing times.

In addition, the distribution of sample mass across the Pareto-optimal results shows a relatively even spread, with a slight tendency toward lower values. Approximately 37 % of the data points are situated within the low SM range of 21.378–24.252 g, highlighting that smaller feedstock quantities more frequently yield favorable trade-offs among CV, FCC, and VMC. This trend can be attributed to more uniform microwave penetration and efficient thermal decomposition at smaller scales. Meanwhile, 33 % of the data occupy the medium SM category of 24.253–27.127 g, suggesting that moderate sample masses also maintain competitive performance, balancing uniform heating with practical processing capacities. The remaining 30 % of data points fall within the high SM range of 27.128–30.0 g. Although less common, larger samples still contribute meaningfully to desirable pyrolysis outcomes under

designed operating conditions. Collectively, this distribution demonstrates that careful selection of feedstock mass is essential to optimize microwave energy absorption and overall product quality.

Regarding nitrogen gas flow rate, categorization of the NGFR data into three practical ranges reveals distinct preferences in the Pareto front. Approximately 51 % of the optimal points are found within the low NGFR range (100–118.17 mL/min), indicating that lower flow rates are generally advantageous for maximizing calorific value and carbon content while minimizing unnecessary energy expenditure. About 35 % of the solutions fall into the medium NGFR range (118.17–136.34 mL/min), reflecting that moderate gas flow conditions also play an important role in achieving balanced pyrolysis outcomes, particularly where a slight increase in process intensity may help reduce residual volatiles without significant energy penalties. The remaining 14 % of data points lie within the high NGFR interval (136.34–154.5 mL/min), suggesting that higher flow rates are less commonly selected as optimal, likely due to increased operational demands and the potential for inefficient heat transfer. Altogether, this categorical breakdown confirms that tuning NGFR within lower to medium ranges generally supports the desired trade-offs in bio-char production quality and energy efficiency.

The observed trade-offs provide valuable insights for industrial deployment of microwave-assisted pyrolysis of PKS. In practice, operators must balance between maximizing calorific value for energy-rich bio-char and enhancing fixed carbon content for structural stability, while keeping volatile matter content low to ensure thermal durability and safety. For example, the tendency of higher FCC and lower VMC to arise under longer reaction times and larger feed masses implies that industries aiming to produce durable carbon-rich materials such as for metallurgical or electrode applications may prioritize these conditions despite a modest reduction in CV. Conversely, energy-focused applications, such as combustion or co-firing, benefit from shorter reaction times and lower feed masses, which maximize CV but yield slightly less carbon stability. Moreover, the preference for low-to-moderate nitrogen flow rates highlights a pathway to reduce operational costs while maintaining desirable product quality. Thus, the Pareto front interpretation supports context-specific optimization aligned with industrial objectives.

To benchmark the realism of the optimization outcomes, the results were compared with the experimental optimum reported by Jamaluddin et al. (Ismail et al., 2013), who identified a reaction time of 31.58 min, sample mass of 30 g, and nitrogen gas flow rate of 100 mL/min. Under these conditions, the calorific value, fixed carbon content, and volatile matter content were 29.9 MJ/kg, 59.8 wt%, and 36.4 wt%, respectively. In contrast, the present MOGWO-based multi-objective optimization identified Pareto-optimal conditions yielding higher performance: CV up to ~31.1 MJ/kg, FCC up to 67.78 wt%, and VMC reduced to ~28.2 wt%. These results indicate an approximate 4 % increase in CV, 13 % increase in FCC, and 22 % reduction in VMC compared with the previous study, demonstrating that the proposed framework can generate more thermally stable and energy-dense bio-char. Additionally, unlike the single-point optimum of Jamaluddin et al., the current approach provides a spectrum of trade-off solutions, allowing for flexible selection of processing conditions based on desired priorities among CV, FCC, and VMC. This comparison confirms the practical feasibility and enhanced performance of the optimized conditions predicted by the proposed framework relative to conventional experimental optimization.

4. Multi-criteria decision-making

In practical engineering scenarios, particularly in the optimization and operation of advanced energy conversion systems, decision-making often entails navigating multiple objectives that naturally compete with one another. This holds true for the design and control of microwave-assisted pyrolysis processes, where maximizing bio-char quality must be balanced with operational efficiency and resource constraints. To address these inherently conflicting goals, robust analytical tools are essential. MCDM techniques have therefore become vital in research and practice, as they provide a structured basis for assessing alternative solutions across diverse performance indicators. In the present study, the Weighted Tchebycheff Method is adopted to tackle this complexity. As a recognized MCDM approach, WTM (Ozbey & Karwan, 2014; Soylu, 2011) enables the systematic ranking of alternative operating scenarios according to varying technical and practical priorities. This technique is especially advantageous for problems involving competing objectives, as it consolidates diverse performance criteria into one comprehensive measure by emphasizing the maximum weighted gap from a desired target. By applying tailored weights to each goal, it enables decision-makers to reflect their specific priorities within the selection process, ensuring that trade-offs align with practical or strategic preferences. The use of this method for ranking Pareto-optimal solutions under different scenarios is demonstrated in Ben Hamida et al. (Ben Hamida et al., 2025).

Table 4 presents a comprehensive set of ten distinct decision-making scenarios (A to J) derived using WTM, each embodying different weighting schemes to systematically explore a spectrum of trade-offs between the key thermal performance objectives of microwave-assisted pyrolysis of PKS. These scenarios, graphically represented along the Pareto front in Fig. 9, exemplify how diverse combinations of weights can be used to design operating conditions in line with varying technical goals and real-world constraints. By doing so, this study delivers a robust decision-support toolkit for practitioners aiming to balance energy efficiency, product quality, and process practicality when converting biomass into high-value bio-char.

Scenario A represents the pure single-objective strategy focused solely on maximizing CV, with full weight given to this parameter. In this configuration, the resulting predicted CV reaches 31.12 MJ/kg, the highest in the set, confirming that when calorific performance is prioritized, the process can deliver maximum heating value, while the FCC and VMC settle at around 65.50 wt% and 31.03 wt%, respectively. This scenario is most relevant for industries interested in maximizing the energy density of bio-char for fuel use in power generation or co-combustion, where higher calorific value directly improves combustion efficiency. Scenario B shifts the focus entirely to maximizing FCC. Under this weighting scheme, the process configuration produces an FCC of approximately 67.78 wt%, which is the highest fixed carbon outcome among all scenarios. The CV and VMC in this case adjust to about 30.39 MJ/kg and 28.30 wt%, respectively, indicating that maximizing carbon retention slightly reduces the achievable energy content but yields a product with superior carbon structure. This is especially valuable for applications such as soil amendment, carbon sequestration, or production of high-grade activated carbon. Scenario C is designed to minimize VMC exclusively. Here, the process achieves the lowest volatile matter level at around 28.23 wt%, with CV and FCC stabilizing at 30.29 MJ/kg and 67.72 wt%, respectively. This scenario suits industries or regulatory environments where reduced volatiles are critical for clean combustion, fewer emissions, or applications where volatile residues could compromise downstream processing, such as in metallurgy or environmental remediation.

Scenarios D, E, and F represent dual-objective trade-offs. Scenario D balances CV and FCC equally, producing a CV of 30.84 MJ/kg, an FCC of 67.05 wt%, and a moderate VMC of 29.26 wt%. This scenario provides a practical middle ground where energy content and carbon density are optimized together, useful for operations that require robust fuel characteristics with stable carbon quality. Scenario E couples CV with VMC, yielding a CV of 30.83 MJ/kg, a slightly reduced FCC of 67.12 wt%, and a VMC lowered to 29.16 wt%. This is an ideal compromise for processes that need both high energy output and reduced volatile emissions. Scenario F emphasizes FCC and VMC, resulting in an FCC of 67.76 wt%, VMC of 28.25 wt%, and CV of 30.32 MJ/kg. This is valuable when maximizing the carbon quality and purity of the product is more critical than maximizing its calorific value.

Scenario G represents an equal-weight, full multi-criteria decision-

Table 4
WTM decision-making scenarios (A–J) with different weighting strategies for CV, FCC, and VMC, illustrating how varying priorities influence the selection of optimal pyrolysis operating conditions.

Scenario	Weight			Input			Target		
	W_{CV}	W_{FCC}	W_{VMC}	CV (MJ/kg)	FCC (wt%)	VMC (wt%)	CV (MJ/kg)	FCC (wt%)	VMC (wt%)
A	1	0	0	38.81	21.38	100.00	31.12	65.50	31.03
B	0	1	0	43.05	30.00	144.02	30.39	67.78	28.30
C	0	0	1	43.04	30.00	154.54	30.29	67.72	28.23
D	1	1	0	41.00	25.81	121.08	30.84	67.05	29.26
E	1	0	1	40.55	26.47	121.99	30.83	67.12	29.16
F	0	1	1	43.20	29.99	149.99	30.32	67.76	28.25
G	1	1	1	40.55	26.47	121.99	30.83	67.12	29.16
H	3	1	1	39.64	24.82	113.46	30.96	66.63	29.74
I	1	3	1	40.89	27.80	130.88	30.70	67.40	28.76
J	1	1	3	41.20	28.25	130.69	30.67	67.48	28.70

making approach, ensuring no single performance goal dominates the others. Here, the outcomes stabilize at a CV of 30.83 MJ/kg, FCC of 67.12 wt%, and VMC of 29.16 wt%, showcasing a well-balanced compromise suitable for general applications where all three quality indicators must be consistently maintained at acceptable levels. Scenarios H, I, and J push the exploration further by introducing a dominant emphasis on one objective while still retaining moderate concern for the other two, mimicking realistic shifts in industrial priorities. Scenario H tilts the balance heavily toward CV, raising it to 30.96 MJ/kg, with FCC at 66.63 wt% and VMC at 29.74 wt%. This is practical for energy-intensive use cases where maximum fuel efficiency is prioritized but a baseline product quality must be preserved. Scenario I flips this balance in favor of FCC, producing an FCC of 67.40 wt%, CV of 30.70 MJ/kg, and VMC of 28.76 wt%. Such a setting is ideal for advanced adsorbents or applications needing stable, high-carbon bio-char for high-end industrial use. Scenario J elevates the weight on minimizing VMC, resulting in a reduced VMC of 28.70 wt%, alongside a CV of 30.67 MJ/kg and FCC of 67.48 wt%. This reflects practical needs where strict environmental standards necessitate low-volatile outputs to meet stringent emission controls or product purity requirements.

Collectively, these scenarios illustrate the critical role of flexible weighting in real-world decision-making. They show that by adjusting the relative importance of CV, FCC, and VMC, process designers and operators can strategically align bio-char production with various operational, economic, and environmental objectives. This diversity is what makes the WTM approach so powerful when paired with a robust Pareto front: rather than converging on a single "best" point, the designer gains a family of equally optimal solutions mapped out across the trade-off space in Fig. 9. In practice, this means that a bioenergy plant operator can, for instance, prioritize maximum fuel value during peak energy demand seasons (Scenario A or H), shift toward higher carbon retention when producing premium-grade carbon products (Scenario B or I), or ensure lower volatiles to comply with emissions caps during sensitive operations (Scenario C or J). The existence of these carefully curated scenarios demonstrates the study's commitment to practical applicability, ensuring that the optimal operating strategies are not theoretical abstractions but actionable configurations that can adapt dynamically to evolving constraints and market demands.

5. Conclusions and future directions

5.1. Study overview

This study has successfully addressed a critical methodological gap in the domain of biomass pyrolysis by developing and demonstrating an innovative hybrid framework that seamlessly integrates advanced machine learning, metaheuristic multi-objective optimization, and systematic MCDM. The primary objective was to model, optimize, and prioritize operating scenarios for microwave radiation-induced pyrolysis of palm kernel shells (PKS), thereby maximizing the efficiency and value of bio-char production under inherently nonlinear and competing performance criteria. The proposed methodology unfolded through a structured four-phase approach: (1) comprehensive data exploration and input-output correlation analysis, (2) predictive surrogate modeling using the COMBI algorithm, (3) simultaneous multi-objective optimization with MOGWO, and (4) final prioritization of optimal solutions via the WTM. This robust integration overcomes fragmented approaches seen in prior studies, delivering a scalable and adaptable decision-support system for sustainable biomass valorization.

5.2. Key findings

The key outcomes of this study can be summarized as follows:

- The COMBI model demonstrated outstanding predictive performance across all critical pyrolysis outputs. For example, the calorific value predictions achieved an exceptionally low testing MAPE of 1.002 %, and a near-perfect R^2 of 0.9986, signifying minimal deviation and excellent generalization to unseen data. Similarly, fixed carbon content and volatile matter content predictions maintained high statistical accuracy ($R^2 > 0.99$) on testing data, reinforcing the reliability of the surrogate models in capturing complex process relationships.
- Optimization outcomes revealed insightful trade-offs among reaction time, sample mass, and nitrogen gas flow rate. Notably, higher calorific values (up to 31.12 MJ/kg) were linked to shorter reaction times and smaller sample masses under lower gas flow rates, whereas maximizing fixed carbon content (up to 67.78 wt%) required longer reaction durations and larger sample masses with elevated gas flows. The resulting Pareto front highlighted that over half of the optimal solutions favored shorter reaction times, while nitrogen flow rate optimization showed a clear preference for low to medium ranges to balance energy input and carbon retention effectively.
- Further refinement through the WTM decision-making framework provided ten distinct operating scenarios, each tailored to different technical and practical objectives. This flexibility highlights the framework's real-world applicability: it equips bioenergy practitioners with a family of actionable, equally optimal solutions, enabling dynamic alignment of pyrolysis operations with shifting market demands, energy needs, or environmental constraints.

5.3. Limitations and future directions

While the proposed framework represents a significant methodological advancement, several limitations warrant consideration. The modeling relied on a specific experimental dataset, which may not capture all possible variabilities of large-scale industrial operations. Moreover, feedstock heterogeneity (arising from differences in moisture content, particle size, and compositional variability) can strongly influence pyrolysis performance and has not yet been fully addressed.

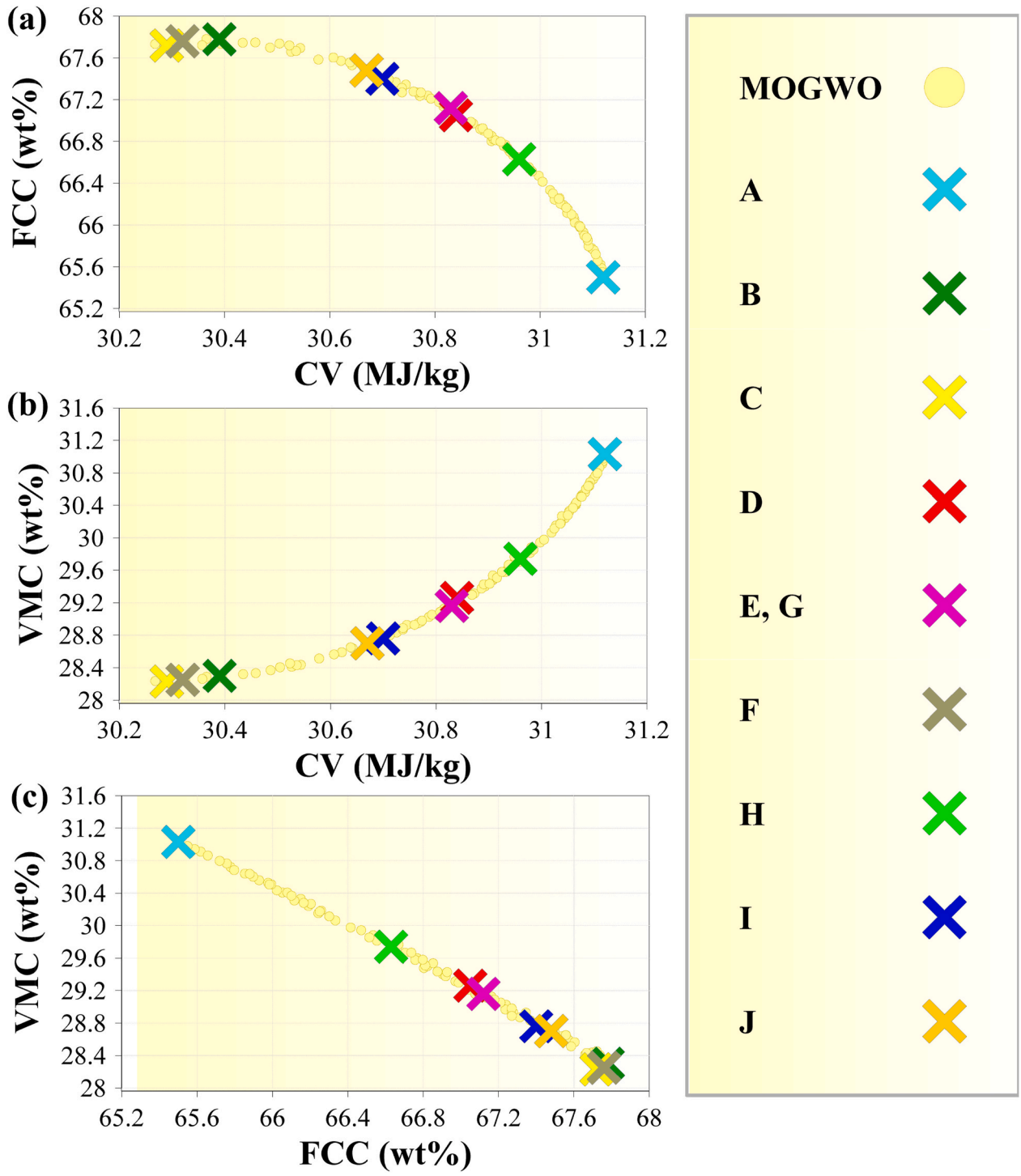

Fig. 9. Distribution of selected operating designs from WTM scenarios (A–J) across the Pareto-optimal trade-offs obtained using MOGWO, showing how different weighting strategies influence CV, FCC, and VMC in the optimized solutions.

Similarly, scale-up challenges, such as non-uniform microwave penetration and heat transfer limitations in larger reactors, could affect the practical transferability of the optimized conditions. The computational demand of integrating metaheuristic optimization with MCDM also poses a challenge, particularly for real-time monitoring and decision-making, where faster surrogate models or reduced-order approaches may be required. Operational safety considerations under industrial conditions remain another area needing systematic investigation. Future research should therefore validate the framework across diverse biomass types, larger-scale reactors, and real-time control settings. Incorporating dynamic process constraints, economic cost analysis, and environmental impact assessments could further enhance the robustness and sustainability of the proposed decision-support system. Ultimately, this hybrid approach holds great promise for optimizing biomass conversion pathways, contributing meaningfully to the global transition toward cleaner and more efficient thermal processing technologies.

CRediT authorship contribution statement

Narinderjit Singh Sawaran Singh: Writing – original draft,

Investigation, Formal analysis, Conceptualization. **Rashid Khan:** Software, Methodology, Formal analysis, Data curation. **As'ad Alizadeh:** Supervision, Software, Resources, Project administration. **Mohamed Shaban:** Writing – review & editing, Validation, Software, Methodology. **Mazen M. Othayq:** Writing – original draft, Software, Formal analysis. **Abdellatif M. Sadeq:** Visualization, Software, Methodology. **Husam Rajab:** Writing – review & editing, Software, Methodology. **Joy Djuansjah:** Writing – original draft, Formal analysis, Conceptualization.

Funding

This work was supported and funded by the Deanship of Scientific Research at Imam Mohammad Ibn Saud Islamic University (IMSIU) (grant number IMSIU-DDRSP2503).

Abbreviations

Artificial Intelligence	AI
Artificial Neural Network	ANN
Calorific Value	CV
Central Composite Rotatable Design	CCRD
Combinatorial Algorithm	COMBI
Fixed Carbon Content	FCC
Gaussian Process Regression	GPR
Grey Wolf Optimizer	GWO
Group Method of Data Handling	GMDH
Machine Learning	ML
Mean Absolute Percentage Error	MAPE
Mean Squared Error	MSE
Microwave-Assisted Pyrolysis	MAP
Multi-Criteria Decision-Making	MCDM
Multi-Objective Grey Wolf Optimizer	MOGWO
Multi-Objective Optimization	MOO
Nitrogen Gas Flow Rate	NGR
Non-Dominated Sorting Genetic Algorithm II	NSGA-II
Palm Kernel Shell	PKS
Pearson Correlation Coefficient	PCC
Predictive Residual Sum of Squares	PRESS
Random Forest	RF
Reaction Time	RT
Response Surface Methodology	RSM
Sample Mass	SM
Support Vector Machine	SVM
Sustainable Development Goal	SDG
Volatile Matter Content	VMC
Weighted Tchebycheff Method	WTM

References

Abdollahi, S. A., Alenezi, A., Alizadeh, A.a., Jasim, D. J., Ahmed, M., Fezaa, L. H., Aich, W., Said, L. B., Kolsi, L., & Maleki, H. (2024a). A novel insight into the design of perforated-finned heat sinks based on a hybrid procedure: Computational fluid dynamics, machine learning, multi-objective optimization, and multi-criteria decision-making. *International Communications in Heat and Mass Transfer, 155*, Article 107535.

Abdollahi, S. A., Basem, A., Alizadeh, A.a., Jasim, D. J., Ahmed, M., Sultan, A. J., Ranjbar, S. F., & Maleki, H. (2024b). Combining artificial intelligence and computational fluid dynamics for optimal design of laterally perforated finned heat sinks. *Results in Engineering, 21*, Article 102002.

Alotaibi, M. A., Alhejaili, W., & Aly, A. M. (2025). ISPH simulation of thermal radiation, soret, and dufour effects on heat and mass transfer in a porous channel with NEPCM and AI integration. *Journal of Radiation Research and Applied Sciences, 18*(3), Article 101698.

Alsehli, M., Basem, A., Mausam, K., Alshamrani, A., Sultan, A. J., Kassim, M., Rajab, H., Musa, V. A., & Maleki, H. (2024). Insights into water-lubricated transport of heavy and extra-heavy oils: Application of CFD, RSM, and metaheuristic optimized machine learning models. *Fuel, 374*, Article 132431.

Alvarado Flores, J. J., Alcaraz Vera, J. V., Ávalos Rodríguez, M. L., López Sosa, L. B., Rutiaga Quiñones, J. G., Pintor Ibarra, L. F., Márquez Montesino, F., & Aguado Zarraga, R. (2022). Analysis of pyrolysis kinetic parameters based on various mathematical models for more than twenty different biomasses: A review. *Energies, 15*(18), 6524.

Alwadai, N., Al Huwayz, M., Alrowaili, Z., Baskin, M., & Al-Buriahi, M. (2024). Predicting the mass attenuation coefficient of glass systems using machine learning approach for radiation applications. *Journal of Radiation Research and Applied Sciences, 17*(2), Article 100919.

An, Y., Tahmasebi, A., Zhao, X., Matamba, T., & Yu, J. (2020). Catalytic reforming of palm kernel shell microwave pyrolysis vapors over iron-loaded activated carbon: Enhanced production of phenol and hydrogen. *Bioresource Technology, 306*, Article 123111.

Ang, W. L., Boon Mee, C. A., Sambudi, N. S., Mohammad, A. W., Leo, C. P., Mahmoudi, E., Ba-Abbad, M., & Benamor, A. (2020). Microwave-assisted conversion of palm kernel shell biomass waste to photoluminescent carbon dots. *Scientific Reports, 10*(1), Article 21199.

Basem, A., Abdulaali, H. K., Alizadeh, A.a., Singh, P. K., Parashar, K., Anqi, A. E., Rajab, H., Cajla, P., & Maleki, H. (2024). Integrating artificial Intelligence-Based metaheuristic optimization with Machine learning to enhance Nanomaterial-Containing latent heat thermal energy storage systems. *Energy Conversion and Management: X, 25*, Article 100835.

Ben Hamida, M. B., Basem, A., Varshney, N., & Mostafa, L. (2025). Intelligent design of high-performance fluids for thermal management: Integrating response surface methodology, weighted tchebycheff method, and strength pareto evolutionary algorithm II. *Scientific Reports, 15*(1), Article 21508.

Blair, M. J., Gagnon, B., Klain, A., & Kulišić, B. (2021). Contribution of biomass supply chains for bioenergy to sustainable development goals. *Land, 10*(2), 181.

Chen, B., Wang, H., Qiu, X., Yin, Z., Sun, H., & Li, A. (2024). Investigation of sawdust microwave-assisted pyrolysis by machine learning, part I: Optimization insights by large language models. *Fuel, 374*, Article 132396.

Divyabharathi, R., Kalidasan, B., Js, S. S. R., & Chinnasamy, S. (2024). Recent advances in sustainable agro residue utilisation, barriers and remediation for environmental management: Present insights and future challenges. *Industrial Crops and Products, 216*, Article 118790.

Elhaie, M., Koozari, A., & Shahbazi-Gahrouei, D. (2025). Machine learning and neural network approaches for enhanced measuring and prediction of radiation doses. *Journal of Radiation Research and Applied Sciences, 18*(1), Article 101252.

Ethaib, S., Omar, R., Kamal, S. M. M., Awang Biak, D. R., & Zubaidi, S. L. (2020). Microwave-assisted pyrolysis of biomass waste: A mini review. *Processes, 8*(9), 1190.

Faris, H., Aljarah, I., Al-Betar, M. A., & Mirjalili, S. (2018). Grey wolf optimizer: A review of recent variants and applications. *Neural Computing & Applications, 30*, 413–435.

Hai, T., Basem, A., Alizadeh, A.a., Sharma, K., Rajab, H., Mabrouk, A., Kolsi, L., Rajhi, W., Maleki, H., & Sawaran Singh, N. S. (2024a). Integrating artificial neural networks, multi-objective metaheuristic optimization, and multi-criteria decision-making for improving MXene-based ionanofluids applicable in PV/T solar systems. *Scientific Reports, 14*(1), 1–21.

Hai, T., Basem, A., Alizadeh, A.a., Sharma, K., jasim, D. J., Rajab, H., Ahmed, M., Kassim, M., Singh, N. S. S., & Maleki, H. (2024b). Optimizing Gaussian process regression (GPR) hyperparameters with three metaheuristic algorithms for viscosity prediction of suspensions containing microencapsulated PCMs. *Scientific Reports, 14* (1), Article 20271.

Hai, T., Basem, A., Alizadeh, A.a., Singh, P. K., Rajab, H., Maatki, C., Becheikh, N., Kolsi, L., Singh, N. S. S., & Maleki, H. (2025). Optimizing ternary hybrid nanofluids using neural networks, gene expression programming, and multi-objective particle swarm optimization: A computational intelligence strategy. *Scientific Reports, 15*(1), 1986.

Idris, S. S., Rahman, N. A., Ismail, K., Mohammed Yunus, M. F., & Mohd Hakimi, N. I. N. (2022). Microwave-assisted pyrolysis of oil palm biomass: Multi-optimisation of solid char yield and its calorific value using response surface methodology. *Frontiers in Chemical Engineering, 4*, Article 864589.

Ismail, K., Ishak, M. A. M., Ab Ghani, Z., Abdullah, M. F., Safian, M. T.-u., Idris, S. S., Tahiruddin, S., Yunus, M. F. M., & Hakimi, N. I. N. M. (2013). Microwave-assisted pyrolysis of palm kernel shell: Optimization using response surface methodology (RSM). *Renewable Energy, 55*, 357–365.

Jha, S., Nanda, S., Zapata, O., Acharya, B., & Dalai, A. K. (2024). A review of systems thinking perspectives on sustainability in bioresource waste management and circular economy. *Sustainability, 16*(23), Article 10157.

Jiang, Z., Liang, Y., Guo, F., Wang, Y., Li, R., Tang, A., Tu, Y., Zhang, X., Wang, J., & Li, S. (2024). Microwave-assisted pyrolysis-a new way for the sustainable recycling and upgrading of plastic and biomass: A review. *ChemSusChem, 17*(21), Article e202400129.

Kaniapan, S., Hassan, S., Ya, H., Patma Nesan, K., & Azeem, M. (2021). The utilisation of palm oil and oil palm residues and the related challenges as a sustainable alternative in biofuel, bioenergy, and transportation sector: A review. *Sustainability, 13*(6), 3110.

Ke, L., Zhou, N., Wu, Q., Zeng, Y., Tian, X., Zhang, J., Fan, L., Ruan, R., & Wang, Y. (2024). Microwave catalytic pyrolysis of biomass: A review focusing on absorbents and catalysts. *npj Materials Sustainability, 2*(1), 24.

Kiehbadroudinezhad, M., Hosseinzadeh-Bandbafha, H., Mabee, W., Nanda, S., Afshari, H., Saeedi, M., Rathgeber, B., & Zoroufchi Benis, K. (2025). Thermochemical pathways coupled with carbon capture for valorizing animal manure: A review. *Biofuel Research Journal, 12*(2), 2373–2397.

Koshulko, O., Koshulko, A., & Onwubolu, G. C. (2014). *Combinatorial (COMBI) algorithm*. Gmdh-methodology And Implementation In C (With Cd-rom).

Lee, M., Lin, Y.-L., Chiueh, P.-T., & Den, W. (2020). Environmental and energy assessment of biomass residues to biochar as fuel: A brief review with recommendations for future bioenergy systems. *Journal of Cleaner Production, 251*, Article 119714.

Liu, Y., As` arry, A., Hassan, M. K., Hairuddin, A. A., & Mohamad, H. (2024c). Review of the grey wolf optimization algorithm: Variants and applications. *Neural Computing & Applications, 36*(6), 2713–2735.

Liu, Z., Xie, M., Zhou, T., Yang, J., Yang, Y., Liu, T., Dai, S., Huang, Q., Cen, Q., & Xiao, P. (2024a). A review on liquid fuel produced from microwave-assisted pyrolysis of plastic waste. *Process Safety and Environmental Protection, 187*, 833–844.

Liu, Y., Ao, W., Fu, J., Siyal, A. A., An, Q., Zhou, C., Liu, C., Zhang, Y., Chen, Z., & Yun, H. (2024b). Microwave-assisted pyrolysis of industrial biomass waste: Insights into kinetic, characteristics and intrinsic mechanisms. *Energy, 306*, Article 132423.

Marzban, N., Psarianos, M., Herrmann, C., Schulz-Nielsen, L., Olszewska-Widdrat, A., Arefi, A., Pecenka, R., Grundmann, P., Schlüter, O. K., & Hoffmann, T. (2025). Smart integrated biorefineries in bioeconomy: A concept toward zero-waste, emission reduction, and self-sufficient energy production. *Biofuel Research Journal, 12*(1), 2319–2349.

Mirjalili, S., Mirjalili, S. M., & Lewis, A. (2014). Grey wolf optimizer. *Advances in engineering software, 69*, 46–61.

Mirjalili, S., Saremi, S., Mirjalili, S. M., & Coelho, L.d. S. (2016). Multi-objective grey wolf optimizer: A novel algorithm for multi-criterion optimization. *Expert Systems with Applications, 47*, 106–119.

Mohd Hamzah, M. A. A., Hasham, R., Nik Malek, N. A. N., Hashim, Z., Yahayu, M., Abdul Razak, F. I., & Zakaria, Z. A. (2022). Beyond conventional biomass valorisation: Pyrolysis-derived products for biomedical applications. *Biofuel Research Journal, 9* (3), 1648–1658.

Narde, S. R., & Remya, N. (2022). Biochar production from agricultural biomass through microwave-assisted pyrolysis: Predictive modelling and experimental validation of biochar yield. *Environment, Development and Sustainability*, 1–14.

Nasir, M., Sadollah, A., Mirjalili, S., Mansouri, S. A., Safaraliev, M., & Rezaee Jordehi, A. (2024). *A comprehensive review on applications of grey wolf optimizer in energy systems*. Archives of Computational Methods in Engineering.

Ozbey, O., & Karwan, M. H. (2014). An interactive approach for multicriteria decision making using a tchebycheff utility function approximation. *Journal of Multi-Criteria Decision Analysis, 21*(3–4), 153–172.

Palla, S., Surya, D. V., Pritam, K., Puppala, H., Basak, T., & Palla, V. C. S. (2024). A critical review on the influence of operating parameters and feedstock characteristics on microwave pyrolysis of biomass. *Environmental Science and Pollution Research, 31*(46), 57570–57593.

Pattnaik, P., Mishra, S., Sharma, A., & Sharma, R. P. (2025). Neural computing analysis of rate coefficients in nanofluid flow over a wedge with nanoparticle aggregation effect: A machine learning approach. *Neural Computing & Applications*, 1–20.

Paudel, P. P., Kafle, S., Park, S., Kim, S. J., Cho, L., & Kim, D. H. (2024). Advancements in sustainable thermochemical conversion of agricultural crop residues: A systematic review of technical progress, applications, perspectives, and challenges. *Renewable and Sustainable Energy Reviews, 202*, Article 114723.

Raje, A., Bhise, A. A., Surya, D. V., & Kulkarni, A. (2024). Understanding the role of CFD in microwave-assisted pyrolysis for biomass conversion. *Journal of Analytical and Applied Pyrolysis*, Article 106477.

Ren, X., Ghazani, M. S., Zhu, H., Ao, W., Zhang, H., Moreside, E., Zhu, J., Yang, P., Zhong, N., & Bi, X. (2022). Challenges and opportunities in microwave-assisted catalytic pyrolysis of biomass: A review. *Applied Energy, 315*, Article 118970.

Saleh, A., Hasanuzzaman, M., Cassidy, H., Dayang, S., & Shahril, M. (2023). An exploration of modified microwave-assisted rapid hydrothermal liquefaction process for conversion of palm kernel shells to bio-oil. *International Journal of Engineering Materials and Manufacture, 8*(2), 36–50.

Sedgwick, P. (2012). Pearson's correlation coefficient. *Bmj, 345*.

Sepehrnia, M., Maleki, H., Hamidi, A., Davoodi, A., & Golmohammadi, H. (2025). Rheological behavior of MWCNT-SnO2/SAE50 hybrid nanolubricant: Experimental evaluation and viscosity prediction using optimized machine learning model. *Alexandria Engineering Journal, 127*, 771–786.

Sepehrnia, M., Maleki, H., Karimi, M., & Nabati, E. (2022). Examining rheological behavior of CeO2-GO-SA/10W40 ternary hybrid nanofluid based on experiments and COMBI/ANN/RSM modeling. *Scientific Reports, 12*(1), 1–22.

Sharma, R. P., Barik, B. K., Kumar, V. V., & Sharma, A. (2025). Illustration of low oscillating magnetic field on sodium alginate-based hybrid nanofluid flow between two revolving disks: An artificial neural network-based study. *Engineering Applications of Artificial Intelligence, 155*, Article 111101.

Sharma, R. P., Praharaj, S., Barik, B. K., Kumar, V. V., Sharma, A., & Mahanta, C. (2024). Neural network-based analysis of thermal and mass transfer in nanofluid flow through a microchannel under pollutant concentration effect. *Multiscale and Multidisciplinary Modeling, Experiments and Design, 8*(7), 313.

Sharma, A., & Sharma, R. P. (2025a). Utilizing neural networks to illustrate the dynamics of viscous fluid flow over curved surface with homogeneous and heterogeneous reactions. *Engineering Applications of Artificial Intelligence, 159*, Article 111629.

Sharma, A., & Sharma, R. P. (2025b). Enhancing heat transfer rate in hybrid nanofluid flow past a stretching sheet: A response surface methodology approach. *Arabian Journal for Science and Engineering*, 1–21.

Sharma, A., Sharma, R. P., Biswas, A., & Ibrahim, S. M. (2025). Exploring the impact of nanoparticle aggregation in parabolic trough solar collectors with a neural network-based predictions for enhanced thermal performance. *Solar Energy Materials and Solar Cells, 293*, Article 113866.

Shen, J., Yan, M., Fang, M., & Gao, X. (2022). Machine learning-based modeling approaches for estimating pyrolysis products of varied biomass and operating conditions. *Bioresource Technology Reports, 20*, Article 101285.

Siddique, I. J., Salema, A. A., Antunes, E., & Vinu, R. (2022). Technical challenges in scaling up the microwave technology for biomass processing. *Renewable and Sustainable Energy Reviews, 153*, Article 111767.

Snoussi, L., Fakhfakh, O., Khedher, M. I., Khouqeer, G. A., Sharma, K., Hosni, F., & Sallah, M. (2025). Comparative analysis of machine learning techniques for estimating dynamic viscosity in various nanofluids for improving the efficiency of thermal and radiative systems. *Journal of Radiation Research and Applied Sciences, 18* (1), Article 101205.

Soylu, B. (2011). A multi-criteria sorting procedure with tchebycheff utility function. *Computers & Operations Research, 38*(8), 1091–1102.

Sulong, R. S. R., Zulkifli, S. E., Hasham, R., & Zakaria, Z. A. (2020). Characterization of pyroligneous acid produced from microwave-assisted treatment of palm kernel shell. *Journal of Physics: Conference Series, 1444*(1), Article 012005. IOP Publishing.

Syed, N. R., Zhang, B., Mwenya, S., & Aldeen, A. S. (2023). A systematic review on biomass treatment using microwave-assisted pyrolysis under PRISMA guidelines. *Molecules, 28*(14), 5551.

Vinay Kumar, V., Sharma, R. P., & Naveen Kumar, R. (2025). The role of time-varying nanofluid flow and particle aggregation on the kinetics of homogeneous and heterogeneous reactions in position-controlled squeezing porous slider. *Proceedings of the institution of mechanical engineers, part N: Journal of nanomaterials, nanoengineering and nanosystems*, Article 23977914251338162.

Yang, Y., Shahbeik, H., Shafizadeh, A., Masoudnia, N., Rafiee, S., Zhang, Y., Pan, J., Tabatabaei, M., & Aghbashlo, M. (2022). Biomass microwave pyrolysis characterization by machine learning for sustainable rural biorefineries. *Renewable Energy, 201*, 70–86.

Zhang, Z., Al-Bahrani, M., Ruhani, B., Ghalehsalimi, H. H., Ilghani, N. Z., Maleki, H., Ahmad, N., Nasajpour-Esfahani, N., & Toghraie, D. (2023). Optimized ANFIS models based on grid partitioning, subtractive clustering, and fuzzy C-means to precise prediction of thermophysical properties of hybrid nanofluids. *Chemical Engineering Journal, 471*, Article 144362.

Zhang, T., Pasha, A. M. K., Sajadi, S. M., Jasim, D. J., Nasajpour-Esfahani, N., Maleki, H., Salahshour, S., & Baghaei, S. (2024). Optimization of thermophysical properties of nanofluids using a hybrid procedure based on machine learning, multi-objective optimization, and multi-criteria decision-making. *Chemical Engineering Journal, 485*, Article 150059.

Zhong, Y., Liu, F., Huang, G., Zhang, J., Li, C., & Ding, Y. (2024). Thermogravimetric experiments based prediction of biomass pyrolysis behavior: A comparison of typical machine learning regression models in Scikit-learn. *Marine Pollution Bulletin, 202*, Article 116361.